textiles

MDPI

Article

Structure–Property Relationships in Periodate Oxidized Cotton Fabrics: Role of Textile Pretreatments

Romeo Pruneanu [1,2], Melinda Pruneanu [2,3,*], Stelian Sergiu Maier [2,3], Vasilica Popescu [2,3], Vasilica Maier [2,3], Viorica Vasilache [4], Daniel Timpu [5] and Diana Elena Ciolacu [6]

1 Faculty of Industrial Design and Business Management, University Doctoral School, "Gheorghe Asachi" Technical University of Iasi, 700050 Iasi, Romania; romeo.pruneanu@student.tuiasi.ro
2 Centre for Research and Innovation in Textiles and Fashion Industry—SMART-Tex-IS, 700050 Iasi, Romania; stelian-sergiu.maier@academic.tuiasi.ro (S.S.M.); vasilica.popescu@academic.tuiasi.ro (V.P.); vasilica.maier@academic.tuiasi.ro (V.M.)
3 Department of Chemical Engineering in Textiles and Leather, "Gheorghe Asachi" Technical University of Iasi, 700050 Iasi, Romania
4 Arheoinvest Center, Department of Exact Sciences and Natural Sciences, Interdisciplinary Research Institute, "Alexandru Ioan Cuza" University, 700506 Iasi, Romania; viorica_18v@yahoo.com
5 Laboratory of Physical Chemistry of Polymers, "Petru Poni" Institute of Macromolecular Chemistry, 700487 Iasi, Romania; dtimpu@icmpp.ro
6 Laboratory of Natural Polymers, Bioactive and Biocompatible Materials, "Petru Poni" Institute of Macromolecular Chemistry, 700487 Iasi, Romania; dciolacu@icmpp.ro
* Correspondence: melinda.pruneanu@academic.tuiasi.ro

Abstract

This study investigates the influence of conventional textile pretreatment and periodate oxidation parameters on the structural modifications and functional properties of woven cotton fabrics. Unlike most studies focused on cellulose pulps or isolated textile fibers, the present work examines how the initial structural state of the textile substrate, determined by its pretreatment history, governs the oxidation pathways. Cotton fabrics were subjected to alkaline scouring (SC), hydrogen peroxide bleaching (BC), and combined scouring–bleaching (SBC), followed by sodium periodate oxidation under controlled conditions. Carbonyl species were quantified analytically and identified by ATR-FTIR spectroscopy, while structural changes were evaluated by X-ray diffraction (XRD). Mechanical properties were assessed using the normalized parameters (Fa/Fa_0 and E/E_0), hydrophilicity by water absorption capacity (WAC), and optical stability by the yellowness index (YI). The results demonstrated that the pretreatments influence the oxidant accessibility and the balance between carbonyl speciation. XRD analysis shows a moderate decrease in crystallinity, indicating partial preservation of the crystalline domains, whereas mechanical properties decrease significantly (35–65%), concomitant with a 25–45% reduction in WAC. These results suggest that the impairment in mechanical and hydrophilic properties is primarily governed by localized C2–C3 bond scission, secondary oxidative reactions, and supramolecular rearrangements, rather than by bulk crystalline loss. The oxidized SC series exhibits higher YI values associated with an increased free aldehyde content, while the BC and SBC fabrics show improved optical stability. Overall, these results demonstrate that pretreatment history governs periodate oxidation pathways and establishes clear structure–property relationship relevant for the controlled functionalization of woven cotton fabrics.

Keywords: cotton cellulose; pretreatments effects; sodium periodate oxidation; ATR-FTIR; XRD; hydrophilicity; mechanical properties; optical properties

Academic Editor: Jiri Militky

Received: 11 February 2026
Revised: 31 March 2026
Accepted: 7 April 2026
Published: 9 April 2026

1. Introduction

In the last decade, research has increasingly focused on the design of advanced functional biomaterials, in which controlled supramolecular organization and interfacial interactions allow for the achievement of designed functional properties [1,2]. The renewability, biodegradability and versatility of cellulose recommend it as an ideal choice for the production of functional materials that are found in a wide range of applications, from the pulp and paper industry to the cosmetics, food, pharmaceutical and, lastly, textile industries. Cellulose-based substrates, such as cotton fabrics, are widely used in textile processing due to their favorable mechanical performance, physiological comfort and large-scale industrial availability [3]. The selective chemical modification of cellulose represents an effective approach for introducing reactive functionalities and tailoring the structural and functional performance of cellulosic substrates.

Controlled chemical modification of cellulose has therefore been extensively explored to introduce new functionalities while preserving the fibrous structure. Among the available oxidation methods, selective oxidation with sodium or potassium periodate continues to attract has received considerable attention due to its high selectivity toward vicinal diols at the C2–C3 positions of anhydroglucose unit (AGU). This reaction leads to cleavage of the C2–C3 bond and the formation of dialdehyde cellulose (DAC) without direct oxidation of the primary hydroxyl group at the C6 position [4–7]. The reaction occurs preferentially in the amorphous regions of cellulose, with limited penetration into crystalline domains, resulting in a topochemical non-uniform distribution of aldehyde groups [8,9].

Such structural specificity regarding oxidation degree and associated changes in mechanical and functional properties, even under comparable experimental conditions, contributes to a wide variability in data reported in the literature [9,10]. Nevertheless, DAC and related oxycelluloses have attracted considerable attention in applications ranging from biodegradable and bioresorbable [11,12] to hemostatic [13–15], antibacterial materials [16], and reactive supports for subsequent functionalization [17–19].

Nevertheless, the literature clearly demonstrates that periodate oxidation is far from a simple or uniform process. A central and still-debated aspect concerns the distinction between free aldehyde groups (-CHO) formed directly by selective periodate oxidation and the development of secondary reactions leading to the coexistence of multiple oxycellulose forms in equilibrium. These include hydrated aldehydes, hemiacetal and hemialdal structures, and carboxyl groups, as well as a variety of intra- and intermolecular interactions, hydrogen-bond network reorganization, and macromolecular chain degradation [11,20–23].

Accurate characterization of functional groups introduced by periodate oxidation therefore remains challenging. Quantification of aldehyde groups using methods based on hydroxylamine hydrochloride [24–26], iodometry, or tetrazolium-type reagents [27,28] are influenced by the steric accessibility of (–CHO) and by their occurrence in hydrated or otherwise masked forms. Similarly, carboxyl group determination by acid–base titration [29], methylene blue adsorption [30], or by complexometric [30], and conductometric methods [31,32] does not allow for differentiation of their origin, which may result either from non-specific secondary oxidation reactions or from deliberate oxidation of aldehydes, most commonly using sodium chlorite [32].

Classical titrimetric, spectrophotometric, and spectroscopic techniques (FTIR, NIR, ^{13}C-NMR) [20,33,34], as well as advanced molecular fractionation and chemometric approaches [33,35], have been widely applied; however, the results obtained are often divergent. Systematic discrepancies between characterization methods have been demonstrated, highlighting the significant influence of secondary reactions on the reported values of the degree of oxidation [36]. These factors contribute to non-uniform interpretations of the

relationship between chemical structure, supramolecular modifications, and the functional properties of oxidized cellulose.

Topochemical studies have shown that oxidation is controlled by oxidant accessibility at the supramolecular level, being initially localized in the amorphous and paracrystalline regions of cellulose, with limited penetration into crystalline domains [5,20,37]. This non-uniform distribution accounts for the wide variability reported in the literature concerning the degree of oxidation and the interpretation of structural and mechanical changes, even under comparable experimental conditions [37].

Most fundamental studies on periodate oxidation have focused on bleached pulps, microcrystalline cellulose, or nanocelluloses, where reagent accessibility is high and diffusional limitations are minimal [19,25,31,34]. In contrast, cotton fabrics exhibit a dense two-dimensional architecture, high packing density, strong interfibrillar interactions, and a complex wet-processing history, and have therefore been far less systematically investigated. Even in studies involving textile materials [38,39], the focus is frequently placed on fibers or yarns, often bleached or mercerized [27–30,40], subjected to selective oxidation with periodate or TEMPO, without considering the cumulative effects of conventional pretreatment steps on subsequent chemical reactivity during selective oxidation, in conjunction with fabric architecture [28,30].

Conventional pretreatments applied to cellulosic textiles, such as alkaline scouring and hydrogen peroxide bleaching, are well known to exert a significant impact on chemical composition, fiber accessibility, and the distribution of amorphous cellulose regions [39,41]. Although the influence of pretreatments on non-selective oxidation in various oxidative systems has been reported [29,32,38], direct correlation with selective oxidation using sodium or potassium periodate remains insufficiently developed for cotton fabrics.

A clear gap therefore exists in the literature regarding how the processing history of cotton fabrics influences selective periodate oxidation and the resulting distribution of carbonyl functionalities. In such cases, delineation of newly formed functional groups becomes ambiguous, and quantification of the degree of oxidation based solely on free aldehyde groups is complicated by the presence of pre-existing functionalities, rendering such an approach inadequate [36].

In this context, the present study investigates the selective oxidation of cotton fabrics with sodium periodate ($NaIO_4$) following conventional textile pretreatment operations, namely alkaline scouring, hydrogen peroxide bleaching, and their combination.

The objective of this study is to highlight the effects of pretreatments performed on cotton fabrics on the performance of periodate functionalization. These pretreatments represent the standard stages of conventional preparation of cotton textiles, carried out in order to remove natural impurities. However, at the same time, a modification in the chemical composition and accessibility of the cellulose is also achieved, with a direct influence on the penetration of oxidants and the selectivity of the oxidation reaction.

Moreover, this study focuses on correlating the balance between free aldehydic, carboxylic and masked carbonyl groups formed during $NaIO_4$ oxidation and the resulting structural and functional modifications of woven cotton fabrics, with particular emphasis on the influence of substrate pretreatment history. To establish direct correlations between the initial structural state of the substrate, the distribution of carbonyl groups, and the functional performance of the material, analytical determinations, spectroscopic and structural analyses, together with evaluations of mechanical, hydrophilic, and optical properties, were performed. This integrated approach enables a coherent interpretation of the structure–property relationships governing selective periodate oxidation in pretreated cotton fabrics.

2. Materials and Methods

2.1. Materials

In this study, a 100% raw cotton fabric supplied by Majutex (Iasi, Romania) was used. The fabric had a plain weave structure, with a warp yarn density of 24 yarns·cm^{-1} and a weft yarn density of 18 yarns·cm^{-1}, a mass per unit area of 127 g·m^{-2}, and an average thickness of 0.38 mm. The constructional parameters were determined in accordance with SR EN ISO 7211-2:2024, Method A [42].

Conventional pretreatment operations were carried out using Lavotan DSU and Contavan GAL (CHT GmbH, Tübingen, Germany), sodium hydroxide (NaOH), sodium carbonate (Na_2CO_3), and hydrogen peroxide (H_2O_2, 35%). Selective oxidation was performed using sodium periodate ($NaIO_4$, purity $\geq$ 99%, Carl Roth GmbH + Co. KG, Karlsruhe, Germany) in acetate buffer solution (pH = 4.0), prepared with glacial acetic acid (CH_3COOH).

For the analytical determination of free aldehyde and carboxyl groups, hydroxylamine hydrochloride (purity $\geq$ 99%, Fluka-Chemie-GmbH, Buchs, Switzerland.), calcium acetate ($Ca(CH_3COO)_2$, purity 99%, Carl Roth GmbH, Karlsruhe, Germany), ethylenediaminetetraacetic acid (EDTA), ammonium hydroxide solution (NH_4OH, 30%), ammonium chloride (NH_4Cl), methyl orange (CHIMREACTIV, Bucharest, Romania), and Eriochrome Black T (purity $\geq$ 99%, Carl Roth GmbH, Karlsruhe, Germany) were used as received, without further purification.

2.2. Methods

2.2.1. Pretreatment Procedures Applied to Cotton Fabric

The raw cotton fabric was subjected to three conventional pretreatment routes:

- Alkaline scouring (SC): liquor ratio (LR) = 30:1; 1% o.w.f. (on weight of fabric) Lavotan DSU, 2% o.w.f. NaOH, and 1% o.w.f. Na_2CO_3; treatment at 98 °C for 60 min.
- Hydrogen peroxide bleaching (BC): LR = 30:1; 6% o.w.f. H_2O_2 (35%), 1.5% o.w.f. Contavan GAL, 2% o.w.f. NaOH, and 1% o.w.f. Lavotan DSU; pH 10; treatment at 98 °C for 45 min.
- Combined alkaline scouring and bleaching (SBC): LR = 30:1; 4% o.w.f. NaOH, 6% o.w.f. H_2O_2 (35%), 2% o.w.f. Lavotan DSU, 1.5% o.w.f. Contavan GAL, and 1% o.w.f. Na_2CO_3; pH 10; treatment at 98 °C for 45 min.

After pretreatment, the samples were thoroughly rinsed with hot distilled water, neutralized in 0.1 M HCl solution for 15 min, rinsed again with distilled water, and dried at room temperature for at least 48 h.

2.2.2. Sodium Periodate Oxidation

The pretreated samples (10 × 10 cm, approximately 4 g) were oxidized using $NaIO_4$ at concentrations of 0.04 and 0.08 mol·L^{-1} (in acetate buffer solution, pH = 4.0), at reaction temperatures of 30 and 40 °C, according to a methodology adapted from the literature [40]. The oxidation reaction was carried out for 4 h under gentle magnetic stirring (300 rpm), with strict temperature control and under dark conditions to limit secondary reactions. After oxidation, the samples were washed three times with cold distilled water and dried at room temperature for a minimum of 48 h.

The experimental plan followed a full factorial design (3 × 2 × 2), including pretreatment type, oxidant concentration, and reaction temperature as factors, resulting in 12 experimental variants. Each variant was prepared in duplicate, as summarized in Table 1.

Table 1. Experimental protocol.

Experiment	Sample Code	Pre-Treatments of Cotton Fabric	$NaIO_4$ Oxidation	
			Concentration (mol L^{-1})	Temperature (°C)
1	SC1	Alkaline Scouring	0.04	30
2	SC2	Alkaline Scouring	0.04	40
3	SC3	Alkaline Scouring	0.08	30
4	SC4	Alkaline Scouring	0.08	40
5	BC1	Peroxide Bleaching	0.04	30
6	BC2	Peroxide Bleaching	0.04	40
7	BC3	Peroxide Bleaching	0.08	30
8	BC4	Peroxide Bleaching	0.08	40
9	SBC1	Combined alkaline scouring and bleaching	0.04	30
10	SBC2	Combined alkaline scouring and bleaching	0.04	40
11	SBC3	Combined alkaline scouring and bleaching	0.08	30
12	SBC4	Combined alkaline scouring and bleaching	0.08	40
References	RC	Raw Cotton	Untreated cotton fabric	
	SC	Alkaline Scouring Cotton	Unoxidized Alkaline Scouring cotton fabric	
	BC	Peroxide Bleaching Cotton	Unoxidized Peroxide Bleaching cotton fabric	
	SBC	Combined scouring and bleaching Cotton	Unoxidized Alkaline Scouring and Peroxide Bleaching cotton fabric	

2.2.3. Determination of Free Aldehyde Groups

The content of free aldehyde groups was determined using a hydroxylamine hydrochloride titrimetric method, followed by titration of the released acid with 0.1 M NaOH solution. All determinations were performed in duplicate, and the results were expressed as mmol·g^{-1} of sample. The free aldehyde group content, $C_{aldehyde}$ (mmol aldehyde groups·g^{-1}), was calculated using Equation (1), according to the procedure described in the literature [17,24]:

$$C_{aldehyde} = \frac{(n - n_0) * C_{NaOH}}{m_{aldehyde}}, \text{mmol g}^{-1} \quad (1)$$

In Equation (1), n represents the volume (mL) of NaOH solution consumed during titration of the sample; n_0 represents the volume (mL) of 0.1 M NaOH solution consumed during titration of the blank; C_{NaOH} is the molar concentration of the standardized NaOH solution (0.1 M); and $m_{aldehyde}$ is the mass of the dried oxidized or non-oxidized samples used for the determination, expressed in grams.

2.2.4. Determination of Free Carboxyl Groups

Carboxyl groups were quantified using a calcium acetate–EDTA complexometric method adapted from the literature [27,29,30]. The samples were treated with a known excess of calcium acetate, and the unconsumed Ca^{2+} ions were titrated with 0.1 M EDTA solution in ammoniacal buffer (pH 10), using Eriochrome Black T as the indicator. The results were expressed as mmol·g^{-1} of sample dried at room temperature for at least 48 h. All determinations were performed in duplicate, and the reported values represent the mean of the obtained results. The carboxyl group content, $C_{carboxyl}$ (mmol carboxyl groups·g^{-1}), was calculated according to Equation (2):

$$C_{carboxyl} = \frac{(n_0 - n) * C_{EDTA}}{m_{carboxyl}}, \text{mmol g}^{-1} \quad (2)$$

In Equation (2), n represents the volume (mL) of EDTA solution consumed during titration of the sample; n_0 represents the volume (mL) of EDTA solution consumed during

titration of the blank; C_{EDTA} is the molar concentration of the standardized EDTA solution (0.1 M); and $m_{carboxyl}$ is the mass of the dried oxidized or non-oxidized samples used for the determination, expressed in grams.

2.2.5. ATR-FTIR Spectral Analysis

FTIR spectra were recorded using a Frontier FTIR spectrometer (PerkinElmer, Waltham, MA, USA) equipped with an attenuated total reflectance (ATR) accessory. Spectra were collected at a resolution of 4 cm^{-1} over the 4000–650 cm^{-1} spectral range, with 64 scans per sample, at room temperature. To account for potential sample heterogeneity, each oxidized fabric sample was analyzed in triplicate at three randomly selected positions. To highlight the changes induced by the chemical operations (alkaline, oxidative and combined treatments) applied to the textile material on the cellulose fibers, the ATR-FTIR spectra were first compared using the PlotFTIR v1.2.1 package [43] in the R language, v4.5.2 [44], then the 1550–1800 cm^{-1} range was subjected to deconvolution using the Fityk v1.3.2 software application [45], and post-processed by the PlotFTIR R package.

2.2.6. Structural Analysis by X-Ray Diffraction (XRD)

Wide-angle X-ray diffraction (XRD) patterns were recorded using a D8 ADVANCE diffractometer (Bruker AXS, Karlsruhe, Germany), equipped with a Cu anode tube (SIEMENS KFL Cu 2K) operating with Cu Kα radiation (λ = 0.1506 nm), a parallel beam geometry with a Gobel mirror, and a dynamic scintillation detector. Measurements were performed in locked coupled scan mode (step scan), at an accelerating voltage of 36 kV and an emission current of 35 mA. Data were collected with a step size of 0.02° and a counting time of 2 s per step. All diffractograms were recorded over the 2θ range of 5–50°, at a working temperature of 24 °C. Data acquisition was carried out using DIFFRAC Plus Commander software, while data processing and evaluation were performed using DIFFRAC.EVA V1.1 and File Exchange (Bruker, AXS GmbH, Karlsruhe, Germany).

To evaluate the crystallinity variations induced by the chemical treatments applied to cotton fabrics, the 5–40 degrees range of Bragg diffraction angles of all XRD diffractograms was subjected to deconvolution using the same Fityk software application. A preliminary investigation on the position and amplitude of the peaks was performed by baseline correction of the XRD records using 4S Peak Filling algorithm of alkahest R package v1.3.0 [46], followed by Whittaker smoothing, and peak identification by thresholding with adjustable signal-to-noise ratio and sliding window (same R package). As a reference for the position, intensity and Miller indices of the peaks in the XRD diffractograms, the characteristic values of Iβ allomorph of native cellulose were used [47].

The degree of crystallinity (X_c, %) was calculated from XRD patterns by summing the areas of the crystalline diffraction peaks and dividing them by the total area of the diffractogram (crystalline and amorphous contributions) [48], according to Equation (3).

$$X_c = \frac{\sum A_{crystalline}}{A_{total}} \times 100, \% \quad (3)$$

In Equation (3), $A_{crystalline}$ represents the cumulative area of the crystalline diffraction reflections; A_{total} includes the area of the crystalline reflections corresponding to the (1 1 0), (1 −1 0), (2 0 0), (0 1 −2) and (0 1 2) planes of cellulose Iβ, as well as the amorphous scattering and the amorphous reflection associated with the (0 1 2) plane. The crystallinity degree (Xc) was calculated from the integrated areas of the crystalline and amorphous contributions obtained from the XRD diffractograms. The obtained crystallinity values are used as comparative structural parameters and are interpreted relative to the corresponding unoxidized reference samples.

2.2.7. Mechanical Properties

Tensile tests were performed in accordance with ISO 13934-1:2013 (strip method) [49] using a universal testing machine SATRA/STM 466 (SATRA, Kettering, United Kingdom). Prior to testing, the samples were conditioned for 24 h at 65% relative humidity (RH). Tensile measurements were carried out in both the warp and weft directions, with three parallel determinations for each condition. To accommodate the reduced sample dimensions, the tensile test procedure was adapted accordingly. The textile specimens had a width of 40 mm and a total length of 100 mm, with a gauge length of 60 mm. The crosshead speed was set to 100 mm·min^{-1}. The maximum tensile force at break (Fa, N) and the elongation at break (E, %) were recorded.

2.2.8. Water Absorption Capacity

Water absorption capacity (WAC) was determined in accordance with ISO 20158:2018 [50]. The procedure was performed in triplicate for each sample type, and the WAC values were calculated using the following equation:

$$WAC = \frac{m_1 - m_0}{m_0} \times 100, \% \quad (4)$$

In Equation (4), m_0 represents the mass of the dry sample, while m_1 corresponds to the mass of the wet sample.

The relative variation in water absorption capacity (ΔWAC, %) of the samples was calculated using Equation (5):

$$\Delta WAC = \frac{WAC_{sample} - WAC_{reference}}{WAC_{reference}} \times 100, \% \quad (5)$$

In Equation (5), the negative ΔWAC values indicate a decrease in water absorption capacity, while positive values indicate an increase in hydrophilicity of oxidized sample relative to the corresponding reference samples.

2.2.9. Yellowness Index

The yellowness index (YI) was determined in accordance with ASTM E313-20 [51] using a Datacolor Spectroflash SF300 spectrophotometer (Datacolor, Lawrenceville, NJ, USA). Colorimetric measurements were performed in the CIE L*a*b* color space, based on the corresponding tristimulus values, under standard conditions using illuminant D65 and a 10° standard observer. The YI was calculated according to Equation (6). The reported values represent the mean of five repeated instrumental measurements.

$$YI = \frac{(1.3013 \cdot X - 1.1498 \cdot Z)}{Y} \times 100 \quad (6)$$

In Equation (6), X, Y and Z are the CIE tristimulus values of the sample, and Y represents the luminance component.

2.2.10. Statistical Analysis

Statistical analysis was performed for each experimental group based on three independent replicates. The results are reported as mean values ± standard deviation (SD). Statistical descriptors were applied to evaluate the reproducibility of the measurements and to support the comparative discussion of mechanical properties and water absorption capacity (WAC). For normalized mechanical parameters (Fa/Fa_0 and E/E_0), the associated uncertainty was calculated as the propagated standard deviation of the ratio (σ_R), derived from the individual standard deviations of the measured parameters (n = 3).

Additionally, oxidation experiments were performed in duplicate for each pretreatment condition, oxidant concentration, and temperature, while the aldehyde and carboxyl group contents were determined analytically using duplicate measurements for each sample, and the reported values correspond to the mean values of these determinations.

3. Results and Discussion

3.1. The Determining Role of Pretreatments on the Molecular Structure of Cotton in Fabrics Oxidized with Sodium Periodate

3.1.1. Analytical Quantification of Newly Formed Functional Groups

To evaluate the chemical modifications induced in the cellulose structure $NaIO_4$ oxidation, the contents of free aldehyde and carboxyl groups were quantitatively determined by analytical methods. Oxidation experiments were carried out on cotton fabrics subjected to three different pretreatment routes, under a constant reaction time of 4 h, using $NaIO_4$ concentrations of 0.04 and 0.08 mol·L^{-1}, and reaction temperatures of 30 and 40 °C.

In order to monitor the progress of $NaIO_4$ oxidation, two indicators were defined. The first indicator reflects the overall degree of chemical modification of cellulose and is represented by the total content of free functional groups (C_{total}), expressed in mmol·g^{-1}. This parameter corresponds to the sum of the contents of free aldehyde ($C_{aldehyde}$) and carboxyl groups ($C_{carboxyl}$) formed during periodate oxidation, as expressed by Equation (7):

$$C_{total} = C_{aldehyde} + C_{carboxyl}, \ \text{mmol g}^{-1} \quad (7)$$

The second indicator, $F_{aldehyde}$, is defined as the ratio between the content of free aldehyde groups ($C_{aldehyde}$) and the total content of free functional groups (C_{total}). This parameter represents a qualitative descriptor that is highly sensitive to the severity of the oxidation conditions ($NaIO_4$ concentration and reaction temperature) as well as to the initial structural state of the cotton fabric. It was calculated according to Equation (8):

$$F_{aldehyde} = \frac{C_{aldehyde}}{C_{total}} \quad (8)$$

Figure 1 illustrates the evolution of the contents of free aldehyde and carboxyl groups, as well as the total content of functional groups, as a function of the applied pretreatment type (Figure 1a), together with the correlation between $F_{aldehyde}$ and C_{total} (Figure 1c).

As shown in Figure 1a, the absolute content of functional groups formed during selective $NaIO_4$ oxidation strongly depends on the applied pretreatment route. The SC series exhibits a progressive increase in free aldehyde content, from 0.25–0.35 mmol·g^{-1} (SC1, SC2) at 0.04 mol·L^{-1} $NaIO_4$, to 0.89 mmol·g^{-1} (SC3, SC4) at 0.08 mol·L^{-1} $NaIO_4$, while the carboxyl content remains relatively low (0.18–1.08 mmol·g^{-1}). Consequently, the total functional group content reaches a maximum of 1.97 mmol·g^{-1} and is mainly governed by the periodate concentration, indicating a selective, predominantly primary oxidation process leading to the formation of DAC.

For the BC series, a more balanced distribution between aldehyde and carboxyl groups is observed. Comparable aldehyde levels (0.24–0.93 mmol·g^{-1}) are accompanied by a moderate increase in carboxyl content (≈20% relative to SC samples), resulting in total functional group contents of 0.8–1.8 mmol·g^{-1}. This behavior reflects enhanced fiber accessibility induced by bleaching, which promotes both primary oxidation and the initiation of secondary reactions.

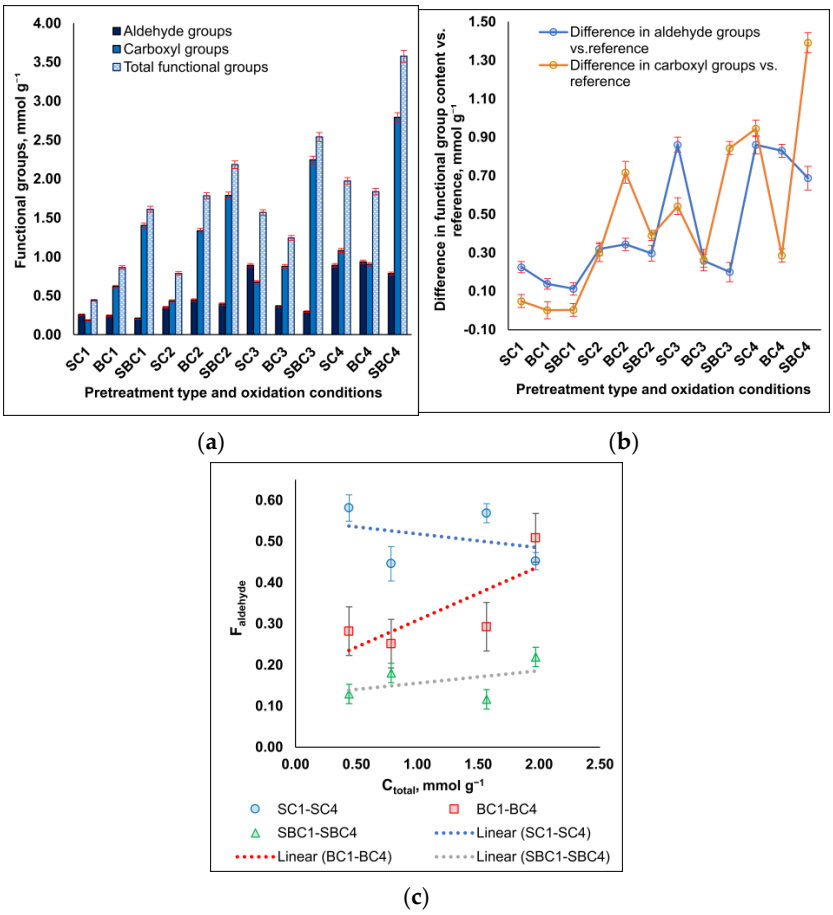

Figure 1. Influence of pretreatment routes and oxidation conditions on the functional group content of $NaIO_4$ oxidized cotton fabrics: (**a**) Variation in free aldehyde, carboxyl, and total functional group content; (**b**) Difference in functional group content relative to the corresponding reference samples; (**c**) Correlation between $F_{aldehyde}$ and C_{total} (dotted lines indicate linear trendlines used only as visual guides to illustrate the general correlation within each pretreatment). Series SC1–SC4, BC1–BC4 and SBC1–SBC4 denote individual samples oxidized with $NaIO_4$ at a concentration of 0.04 and 0.08 mol·L^{-1}, at 30 and 40 °C.

The cumulative effect of alkaline scouring and bleaching is most evident for the SBC oxidized series, which exhibits the highest total functional group contents, reaching up to 3.5 mmol·g^{-1} at 0.08 mol·L^{-1} $NaIO_4$ and 40 °C. Under these conditions, aldehyde levels remain relatively low (0.29–0.78 mmol·g^{-1}) and are mainly temperature-dependent, whereas carboxyl groups increase markedly (1.4–2.79 mmol·g^{-1}), indicating an advanced oxidation regime. For the SBC4 sample, the carboxyl content increases by 120–150% relative to the reference fabric, while the aldehyde content increases by only 40–60%.

As shown in Figure 1b, the difference in functional group content relative to the corresponding reference samples reflects the effect of oxidation severity within each pretreatment route. At 0.04 mol·L^{-1} $NaIO_4$ (series 1 and 2), aldehyde formation predominates, particularly for the SC and BC series, indicating dominant selective C2–C3 cleavage of the AGU, with a slight increase in the carboxyl contribution at 40 °C (BC2), indicating the onset of secondary oxidation. At 0.08 mol·L^{-1} $NaIO_4$ (series 3 and 4), aldehydes dominate at 30 °C, whereas increasing the temperature to 40 °C shifts the reaction pathway toward carboxyl accumulation, most clearly for SBC4. Overall, oxidation conditions modulate reaction severity, while pretreatment governs the dominant functional group evolution.

The relationship between $F_{aldehyde}$ and C_{total} (Figure 1c) highlights distinct oxidation regimes governed by the pretreatment history of the substrate rather than a strict linear correlation. The dotted trendlines are included only as visual guides to illustrate the general tendencies within each pretreatment series. The SC1–SC4 series shows high and relatively constant $F_{aldehyde}$ values (0.45–0.58), characteristic of predominantly selective oxidation. In contrast, the BC series exhibits an increasing trend of $F_{aldehyde}$ with C_{total}, reflecting competition between aldehyde formation and consecutive oxidation to carboxyl groups. The SBC series displays low $F_{aldehyde}$ values (0.13–0.25) and only weak dependence on C_{total}, consistent with advanced oxidation dominated by carboxyl (-COOH) accumulation. Overall, these trends indicate that the pretreatment history governs the oxidation pathway, with SC fabrics favoring selective dialdehyde formation, BC fabrics exhibiting competing oxidation pathways, and SBC fabrics approaching an advanced oxidation regime characterized by increased carboxyl formation. In this context, $F_{aldehyde}$ serves as a robust indicator of the oxidation mechanism, enabling differentiation between selective, competitive, and advanced regimes. Pretreatment governs oxidation progression, whereas oxidation conditions determine its severity.

3.1.2. Structural Investigations by ATR-FTIR Spectral Analysis

ATR-FTIR spectroscopy technique was used to analyze carbonyl-related chemical changes in cotton cellulose induced by pretreatment and periodate oxidation.

Figure 2 presents a comparative overview of the raw ATR -FTIR spectra of the reference samples and all the oxidized sample series, as a function of pretreatment type and oxidation conditions.

Molecular structural characterization based on the ATR-FTIR spectra presented in Figure 2 highlights the structural modifications induced by conventional pretreatment routes and subsequent periodate oxidation of cotton fabrics. The main absorption bands observed in all spectra can be assigned as follows:

- The 3300–3400 cm^{-1} domain is attributed to ν(O–H) stretching vibrations of hydrogen-bonded hydroxyl groups, shows reduced intensity and band broadening for oxidized samples (Figure 2b,c) compared to the reference (Figure 2a) confirms the progression of periodate oxidation, and indicate the disruption of the hydrogen-bond network, resulting in partial amorphization of the cellulose structure [11,41,52].
- In the 2850–2900 cm^{-1} domain, changes in the ν(C–H) stretching profile are observed upon oxidation, consistent with C2–C3 bond cleavage and conformational reorganization of cellulose chains following selective periodate oxidation [11,33].
- Bands at 1150–1160 cm^{-1} and 1030–1050 cm^{-1} are assigned to the asymmetric stretching vibrations ν(C–O–C) of β-(1→4) glycosidic linkages and pyranose ring deformations, respectively [41,52]. Pronounced changes are observed particularly for the SC4, BC4, and SBC4 samples (Figure 2c), reflecting increased structural perturbations under more severe oxidation conditions.
- In the 890–860 cm^{-1} region, increased intensity and band narrowing associated with ν(C–H) deformation vibrations of the glucopyranose ring are observed [11,41], particularly for the BC3, BC4 and SBC3, SBC4 series. These features suggest intrachain rearrangements without extensive polymer backbone degradation and may also include contributions from hemiacetal ν(C=O)–H vibrations formed through secondary reactions of periodate generated aldehyde groups. The evolution of this spectral region is commonly associated with increased supramolecular disorder and is therefore considered an indicator of the relative expansion of amorphous domains within the cellulose matrix [11,35].

- The carbonyl region (1550–1800 cm^{-1}), assigned to ν(C=O) stretching vibrations [41,52], appears as a weak shoulder exclusively in oxidized samples subjected to bleaching or combined alkaline scouring–bleaching pretreatments. At periodate concentrations of 0.04–0.08 $mol \cdot L^{-1}$ and 40 °C, this feature reflects the heterogeneous distribution of oxidation products and is more pronounced for the BC2 and SBC2 (Figure 2b) and BC3–BC4/SBC3–SBC4 series (Figure 2c).

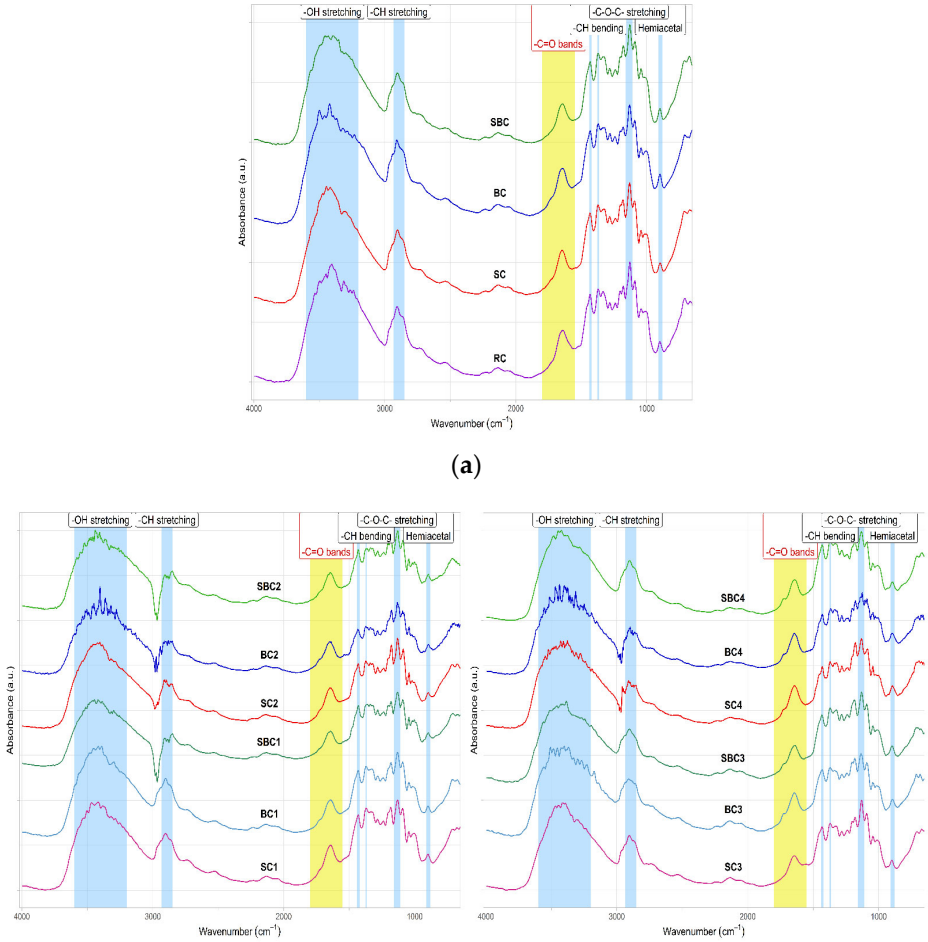

Figure 2. ATR-FTIR spectra recorded for: (**a**) reference cotton fabric samples subjected to the three pretreatment routes; (**b**) samples oxidized with $NaIO_4$ at a concentration of 0.04 $mol \cdot L^{-1}$, at 30 and 40 °C; and (**c**) samples oxidized with $NaIO_4$ at a concentration of 0.08 $mol \cdot L^{-1}$, at 30 and 40 °C. The colored lines represent the different samples within each series, including both reference and corresponding oxidized samples. The shaded regions indicate characteristic absorption bands, such as O–H stretching (~3300–3400 cm^{-1}), C–H stretching (~2850–2900 cm^{-1}), H–O–H bending (~1630–1640 cm^{-1}), carbonyl-related bands (~1550–1800 cm^{-1}), C–O–C stretching vibrations (~1150–1160 cm^{-1}) and ν(C–H) deformation vibrations (~890–860 cm^{-1}), associated with the glucopyranose ring and possible hemiacetal formation.

Given the overlap of ATR -FTIR signals in the carbonyl region and the closely spaced absorption positions of carbonyl species, spectral deconvolution using Voigt functions was applied to achieve more accurate separation and assignment of carbonyl components. The normalized spectra were deconvoluted in the 1800–1550 cm^{-1} region, where carbonyl related absorptions partially overlap and prevent reliable discrimination of individual contributions in the normalized spectra. In particular, the ν(C=O) band characteristic of free aldehyde groups (1730–1740 cm^{-1}) partially overlaps with adjacent carboxyl related

absorption developing in the 1650–1730 cm^{-1} range, leading to band broadening and masking of individual components. The deconvolution procedure enables separation of these overlapping bands and allows for qualitative assessment of the relative evolution of aldehyde, carboxylic, and lactone related absorptions as a function of pretreatment and oxidation severity.

Figure 3 compares the deconvoluted ATR-FTIR spectra of the reference and oxidized samples, highlighting oxidation-induced changes in the distribution of carbonyl-band distribution.

Table 2 summarizes the absorption band ranges identified by deconvolution of the ATR-FTIR spectra (Figure 3) in the 1550–1800 cm^{-1} domain for periodate oxidized cotton samples, corresponding to different pretreatment routes (SC, BC, and SBC) and oxidation levels. This spectral region is particularly relevant for highlighting carbonyl transformations induced by selective cellulose oxidation and governed by the pretreatment history of the cellulosic substrate.

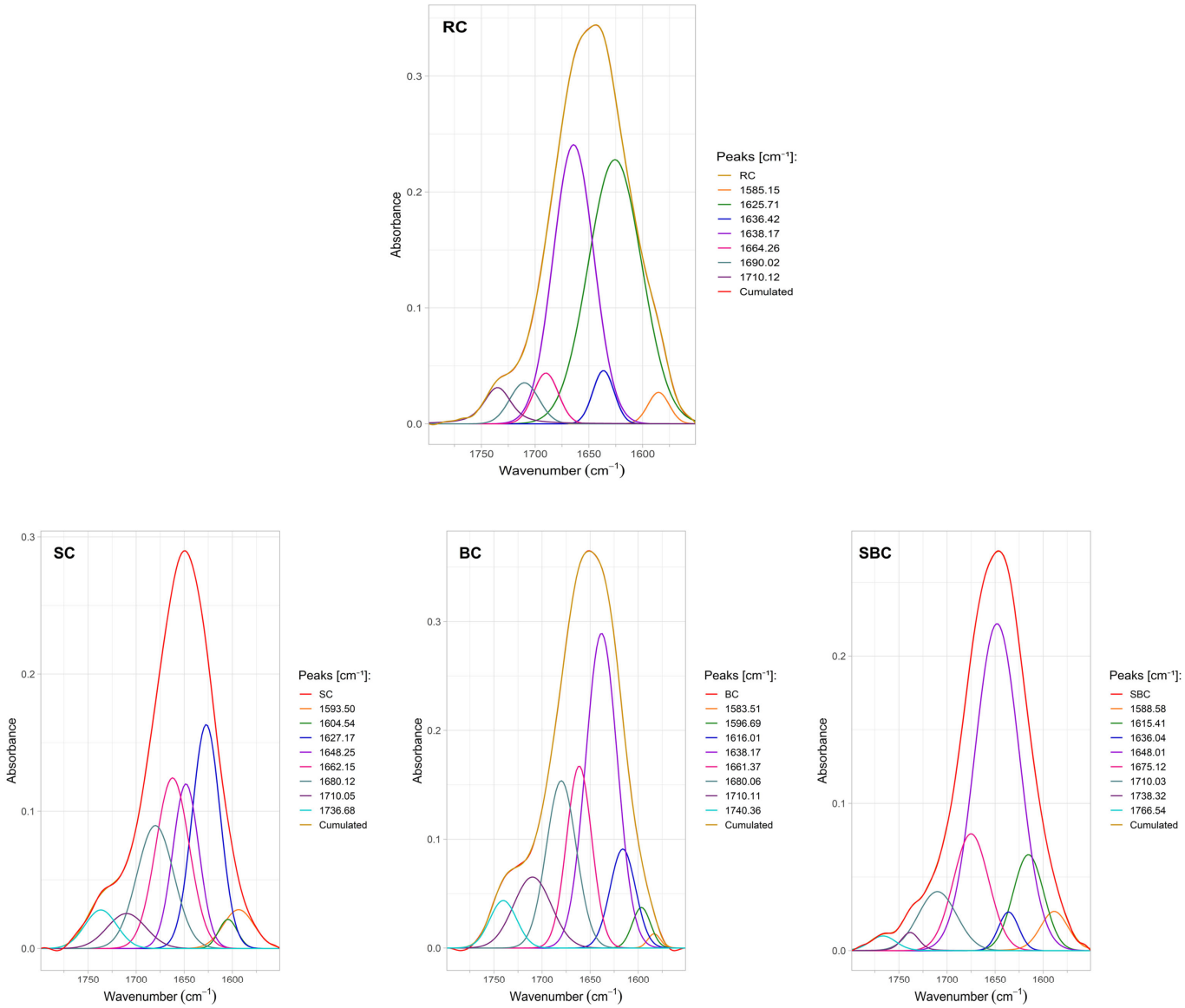

Figure 3. *Cont.*

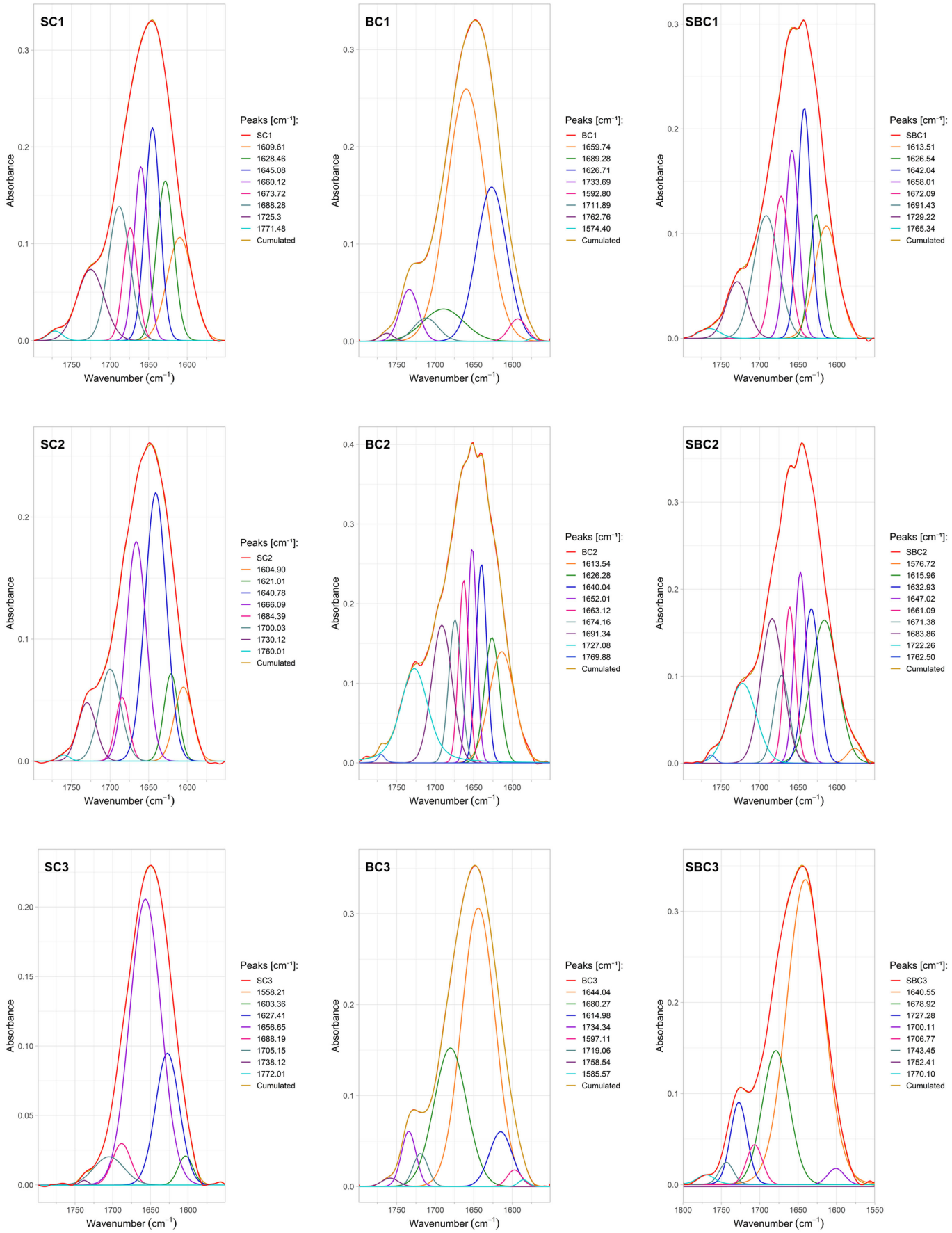

Figure 3. *Cont.*

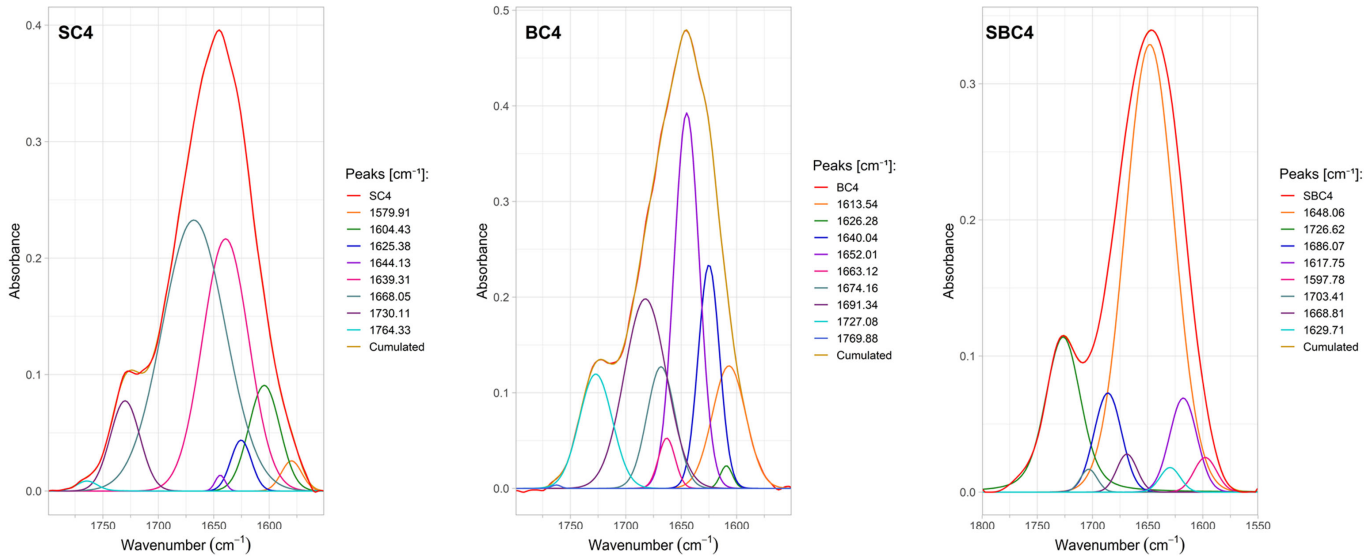

Figure 3. Deconvolution of ATR-FTIR spectra in the 1550–1800 cm^{-1} range for cotton fabric samples subjected to different pretreatment routes and oxidized with $NaIO_4$ at concentrations of 0.04 and 0.08 $mol \cdot L^{-1}$, at temperatures of 30 and 40 °C. The deconvoluted spectrum, the individual Voigt components and the cumulative fitted curve are identified by color in the legend, while the corresponding peak positions are summarized in Table 2.

Table 2. Assignment of ATR-FTIR absorption bands in the 1550–1800 cm^{-1} range for reference samples and $NaIO_4$ oxidized cotton samples.

Sample	Absorption Band, cm^{-1}				
	1550–1630 -C=O (-COO^-— Carboxylate)	**1630–1650 Adsorbed Water δ(H-O-H)**	**1650–1730 -C=O (-COOH—Carboxyl)**	**1730–1740 -C=O (-CHO— Free Aldehyde)**	**1760–1770 -C=O Lactone**
RC	1585; 1625	1636	1664; 1690; 1710	1734	-
SC	1591; 1603	1631	1654, 1674; 1680; 1710	1736	-
BC	1583; 1596; 1616	1638	1661; 1680; 1710	1740	-
SBC	1588; 1615	1636; 1648	1675; 1710	1738	1766
SC1	1609; 1628	1645	1725	-	1771
BC1	1574; 1592; 1626	-	1659; 1689; 1711	1733	1762
SBC1	1613; 1626	1642	1658; 1672; 1691	1729	1765
SC2	1604; 1621	-	1651; 1666; 1684; 1700	1740; 1730	1760
BC2	1591; 1625	1639	1663; 1697; 1726	1729	1769
SBC2	1576; 1615	1632; 1647	1661; 1671; 1683; 1722	-	1762
SC3	1558; 1603; 1627	-	1656; 1705	1738	1772
BC3	1588; 1610; 1624	1646	1671; 1687; 1704; 1726	-	-
SBC3	1600	1640	1678; 1706; 1727;	1743	1770
SC4	1579; 1604; 1625	1639; 1644	1668	1730	1764
BC4	1606; 1609; 1625	1645	1663; 1668 1682; 1727-	-	1762
SBC4	1597; 1617; 1629	1648	1668; 1686; 1703; 1726	-	-

According to the deconvoluted spectra (Figure 3) and the data from Table 2 related to control and oxidized samples, the following spectral domains can be identified: carboxylate groups absorbing in the 1550–1630 cm^{-1} region through asymmetric stretching vibrations ν(–COO^-) [5,34], carboxylic acids in the 1650–1730 cm^{-1} region via ν(C=O) stretching vibrations [34,41], adsorbed water around 1630–1650 cm^{-1} corresponding to δ(H–O–H) bending vibrations [22], free aldehydes characteristic of DAC at 1730–1740 cm^{-1} through ν(C=O) stretching [35], and lactone structures at higher wavenumbers, typically 1760–1770 cm^{-1} [36,53,54].

The deconvoluted ATR-FTIR spectra reveal that the pretreatment route strongly governs the nature and evolution of carbonyl-related species formed during periodate oxidation.

The band located at 1630–1650 cm^{-1} is attributed to the bending vibration δ(H–O–H) of absorbed water [53,54]. The attenuation or disappearance of this band in most oxidized samples indicates a decrease in the surface hydrophilicity of the samples. It is well known that periodate oxidation of cellulose converts the hydrophilic -OH groups at the C2 and C3 positions of the AGU into -CHO groups, leading to the formation of DAC [22]. This structural modification significantly reduces the hydrophilicity of the material, as the resulting aldehyde groups can form intra-and inter-molecular hemiacetal linkages, which are less hydrophilic than the original hydroxyl groups.

In the SC series (alkaline scouring), the spectral response is dominated by the appearance of the 1730–1740 cm^{-1} band, characteristic of free aldehydes (–CHO), while contributions in the 1650–1730 cm^{-1} region associated with carboxylic acids remain limited. This behavior indicates that scouring promotes selective oxidation, leading predominantly to the formation of DAC, with comparatively restrained secondary oxidation.

In contrast, the BC series (bleached samples) exhibits a more complex carbonyl pattern. Alongside the aldehyde band at 1730–1740 cm^{-1}, increasingly intense and broadened absorptions appear in the 1650–1730 cm^{-1} region, corresponding to the stretching vibrations of carboxylic acid groups (-COOH). With increasing oxidation severity, the aldehyde band weakens or disappears, while carboxylic contributions become dominant, indicating a shift from aldehyde formation toward secondary oxidation pathways facilitated by the increased structural accessibility of the cellulose following the bleaching treatment.

The most pronounced changes are observed in the SBC series (scouring and bleaching). These samples display early development of carboxylate and carboxylic acid bands (1550–1650 cm^{-1} and 1650–1730 cm^{-1}, respectively), together with a rapid attenuation of the free aldehyde band at 1730–1740 cm^{-1} under increased oxidation conditions. At advanced oxidation stages, SBC samples also exhibit the most consistent presence of the 1760–1770 cm^{-1} band, evidencing the formation of cyclic lactone structures through intramolecular esterification reactions.

Overall, the ATR-FTIR data demonstrate a clear progression in carbonyl speciation as a function of pretreatment: SC favors selective aldehyde formation, BC promotes partial conversion to carboxylic acids, while SBC accelerates secondary oxidation and lactonization, driving the system toward more stable, oxidized carbonyl structures.

3.1.3. Structural Modifications in Crystallinity Evaluated by X-Ray Diffraction

The crystallinity of the reference samples and of the $NaIO_4$-oxidized ones was evaluated by X-ray diffraction (XRD) analysis. The obtained diffractograms for all samples are presented in Figure 4.

The XRD diffractograms reveal the characteristic cellulose Iβ structure for all samples, with dominant reflections at 2θ values of approximately 14–16°, 22–23°, and 34–35°, corresponding to the crystallographic planes (1 −1 0), (1 1 0), (2 0 0), and (0 0 4).

The crystallographic assignment of the diffraction peaks was performed according to the idealized diffraction patterns of cellulose polymorphs reported by French [55], consistent with the cellulose Iβ structure typical of native cotton fibers described by Nishiyama [4] and Murthy [47]. Structural changes induced by periodate oxidation, including C2–C3 cleavage within the AGU and partial disruption of crystalline order, were interpreted based on previous studies on DAC [5,11,21].

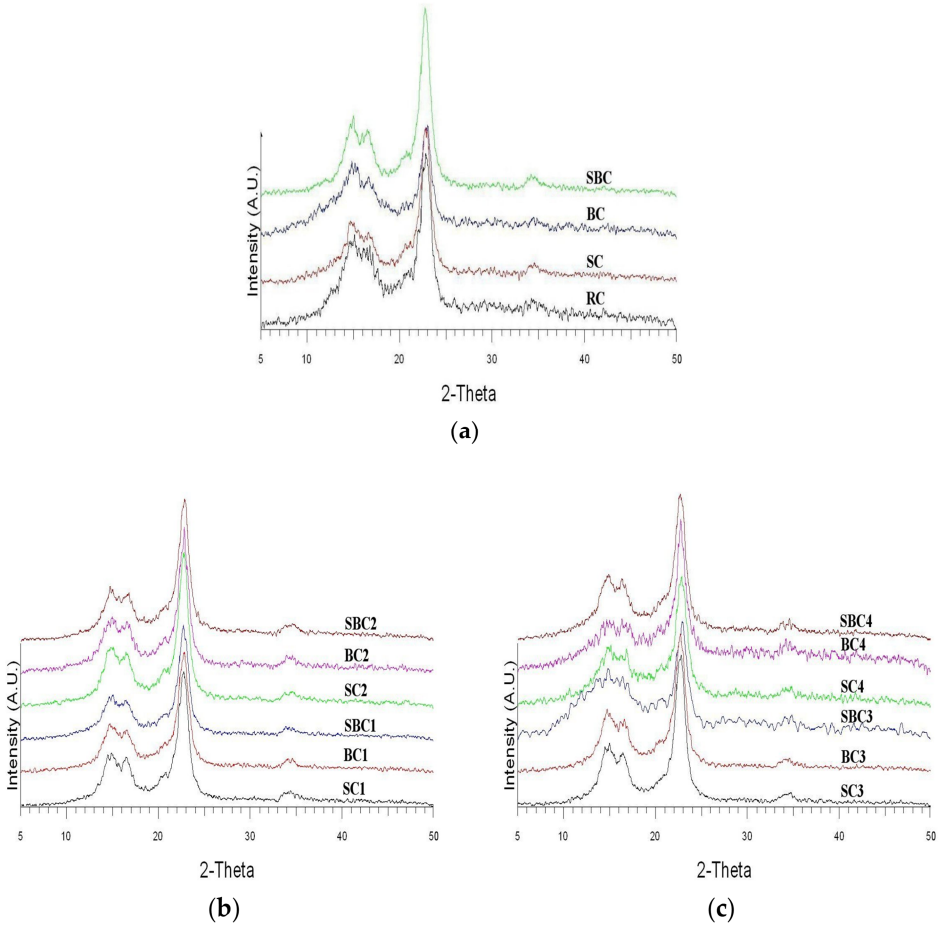

Figure 4. XRD diffractograms recorded for cotton fabric samples subjected to the three pretreatment routes and subsequently oxidized with $NaIO_4$: (**a**) XRD patterns of the reference samples; (**b**) XRD patterns of samples oxidized at a $NaIO_4$ concentration of 0.04 mol·L^{-1} at 30 and 40 °C; and (**c**) XRD patterns of samples oxidized at a $NaIO_4$ concentration of 0.08 mol·L^{-1} at 30 and 40 °C.

In the case of the reference and conventionally pretreated but non-oxidized samples (Figure 4a), variations in the intensity and width of the reflections are observed across the entire range of crystalline planes. For the oxidized samples (Figure 4b,c), the relative intensity of the (2 0 0) reflection progressively decreases, accompanied by an increase in the amorphous background, suggesting partial disruption of the crystalline domains. This effect is more pronounced for samples subjected to combined pretreatment, particularly the SBC series at higher oxidant concentrations and elevated reaction temperatures.

For the evaluation of structural and crystallinity changes in cotton cellulose in various chemically treated textile fabrics, the contributions of the areas corresponding to the crystalline and amorphous phases were compared based on the deconvolution of XRD diffractograms. In order to realistically estimate the amorphous domains, where necessary, both the amorphous background in the 5–40° range and the halo at the base of the peak corresponding to the (2 0 0) plane, which covers the peaks specific to the (0 1 2) and (1 0 2) planes and their reflections, were considered. Explicitly separating the three amorphous contributions in the deconvolution procedure prevents overestimation of the crystalline phase and allows for a more accurate estimation of the total amorphous fraction, avoiding the erroneous assignment of broad amorphous reflections as crystalline reflections [43,49]. As representing the crystalline phase, only the prominent peaks of the (1 −1 0), (1 1 0) and (2 0 0) planes were taken into account for the XRD spectra of all analyzed samples (raw cotton control, scoured, bleached and combined treated fabrics).

The diffractograms of the investigated samples are illustrated in Figure 5 and include the deconvoluted diffraction peaks obtained for both the reference and oxidized samples.

As shown in Figure 5, the diffraction intensity is expressed as counts per second (CPS), representing the raw instrumental signal recorded by the detector as a function of the Bragg diffraction angle (2θ).

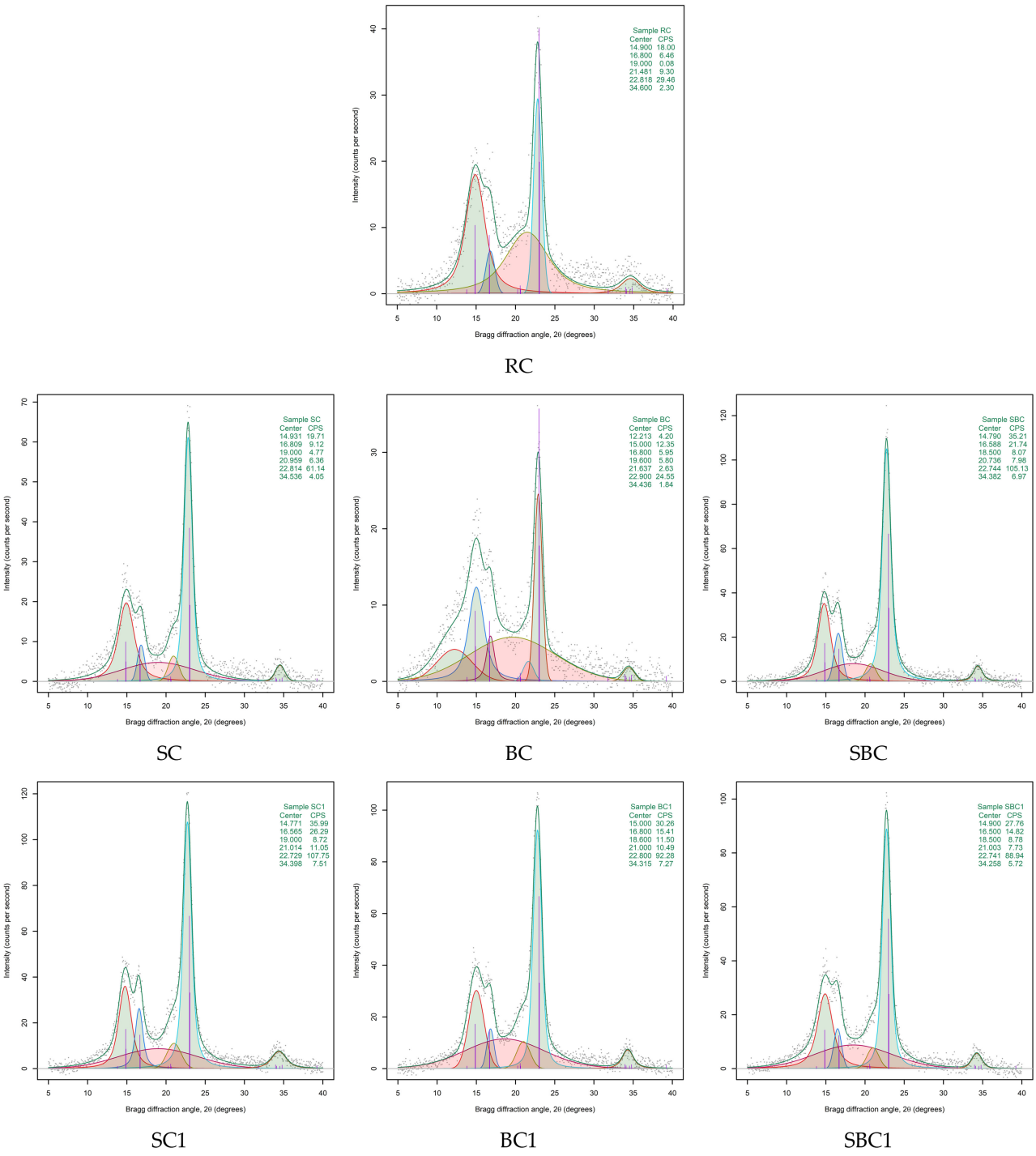

Figure 5. *Cont.*

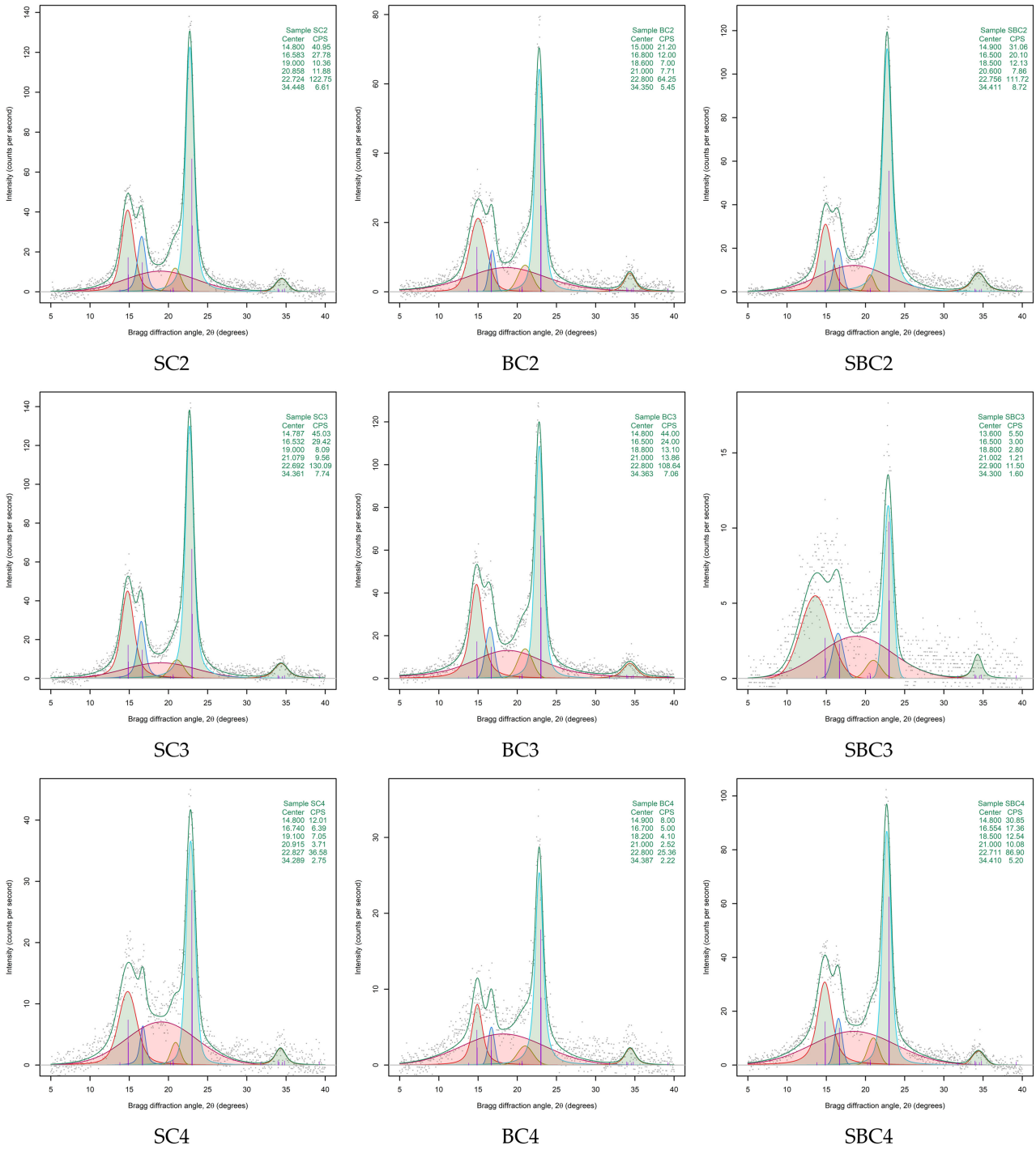

Figure 5. Deconvolution of XRD diffractograms obtained for cotton fabric samples subjected to the three pretreatment routes and oxidized with $NaIO_4$ at concentrations of 0.04 and 0.08 mol·L^{-1}, at reaction temperatures of 30 and 40 °C. The grey dots represent the experimental data, the solid line corresponds to the overall fitted profile, and the individual colored curves represent the deconvoluted peaks (the green shaded areas indicate the crystalline contributions, while the red shaded areas correspond to the amorphous contribution obtained from the deconvolution of the XRD patterns).

Diffraction peaks are identified at 2θ angles of 14.85–14.89°, 16.66–16.71°, 20.27°, 20.59–20.64°, and 22.98–23.04°, characterized by the corresponding Miller indices and assigned to the crystallographic planes (1 −1 0), (1 1 0), (0 1 −2), (0 1 2), and (2 0 0), respectively. The same crystalline planes were identified for all analyzed samples, confirming the preservation of the cellulose Iβ allomorph structure [2,5,21,55].

The diffractograms of all samples exhibit the three expected morphological components. The amorphous scattering evidenced by the broad diffuse background is associated with disordered cellulose chains and their conformational rearrangements. A peculiar amorphous reflection is represented by a broad, poorly defined maximum superimposed in the vicinity of the crystalline (0 1 2) reflection, being attributed to residual order or incomplete chain orientation within paracrystalline and amorphous regions [55,56].

Table 3 summarizes the values of the degree of crystallinity (X_c), calculated according to Equation (3), which directly reflect the structural changes induced by the pretreatment route and by the mechanism of periodate oxidation of cotton fabrics.

Table 3. Degree of crystallinity (X_c) of references and samples subjected both to the three pretreatment routes and the $NaIO_4$ oxidation.

Sample	Area [1 −1 0] Peak	Area [1 1 0] Peak	Area [2 0 0] Peak	Area Amorphous Scattering (Wide Upward Displacement)	Area Amorphous Reflection (Around [0 1 2])	X_c [%]
RC	46.51	19.66	66.09	31.79	13.65	74.43
SC	68.68	9.18	99.75	54.32	10.69	73.21
BC	65.85	5.19	36.36	61.79	5.19	61.59
SBC	25.22	21.02	83.14	79.89	16.06	57.42
SC1	93.04	42.12	185.02	110.08	25.18	70.30
BC1	74.67	17.63	169.61	151.1	22.61	60.12
SBC1	27.76	14.82	145.02	128.16	11.86	57.26
SC2	96.99	43.87	202.83	119.23	26.48	70.23
BC2	64.53	12.68	103.59	102.95	17.78	59.96
SBC2	76.93	27.86	213.91	223.6	14.72	57.22
SC3	118.1	47.1	218.96	142.18	21.3	70.15
BC3	117.49	33.68	174.02	192.43	32.38	59.13
SBC3	12.12	16.04	17.48	40.15	0.93	52.63
SC4	43.49	2.91	60.6	80.23	5.97	55.38
BC4	17.63	5.06	42.26	54.57	6.34	51.60
SBC4	94.4	20.55	120.7	197.9	34.92	50.30

The reported Xc values (Table 2) represent the relative crystalline fraction of each sample in its actual chemical state, enabling direct comparison between raw (RC), pretreated (SC, BC, SBC) and oxidized fabrics (SC1–SC4, BC1–BC4, SBC1–SBC4).

The reference sample (RC) exhibits a high degree of crystallinity (X_c = 74.43%), characteristic of native cellulose Iβ, with well-ordered microfibrils and a stable hydrogen-bond network. Alkaline scouring (SC) does not significantly modify the X_c (73.21%), as this process is dominated by the removal of non-cellulosic impurities without affecting the crystalline domains. Under moderate oxidation conditions (SC1–SC3), the limited decrease in X_c to approximately 70% is attributed to selective oxidation and C2–C3 bond cleavage occurring in the more accessible regions of cellulose, concomitant with relaxation of the hydrogen-bond network and a modest increase in the amorphous phase contribution, without destruction of the crystallites. Under more severe oxidation conditions (SC4—0.08 mol·L^{-1} $NaIO_4$ and 40 °C), a pronounced decrease in X_c to 55.38% is observed, corresponding to a reduction of approximately 24% relative to the SC reference sample. This behavior is associated with advanced oxidation and secondary reactions leading to the formation of masked aldehyde forms (aldehyde hydration, further oxidation to carboxyl groups, and local chain scission), which result in a diminution of the crystalline regions.

Bleaching pretreatment (BC), which itself represents a non-selective oxidation process, leads to initially lower X_c values (61.59% for BC), as a consequence of the removal of non-cellulosic components, partial oxidation of hydroxyl groups, and relaxation of the

hydrogen-bond network. These structural modifications increase the internal accessibility into the fiber, enlarge the amorphous regions and promote oxidant diffusion/exposure, concluded with the cleavage of the C2–C3 bond within the AGU. Oxidation under milder conditions (0.04 mol·L^{-1} $NaIO_4$ at 30 and 40 °C) does not directly affect the crystalline structure, which remains relatively stable, with X_c values in the range of 59.13–60.12% (BC1–BC3 series). In contrast, more severe oxidation conditions (0.08 mol·L^{-1} $NaIO_4$ at 40 °C) lead to a decreased X_c value, of 51.60% for sample BC4, associated with the pronounced development of secondary reactions and a reduction in crystalline domains, overall resulting in a X_c approximately 16% lower than that of the BC reference sample.

The SBC series exhibits the lowest X_c values, with 57.42% for the reference sample and 57.26% (SBC1) and 57.22% (SBC2) under mild oxidation conditions with $NaIO_4$, indicating negligible variation. However, increasing oxidant concentration and temperature results in a X_c reduction of up to 12% (SBC4) relative to the reference sample. These X_c values indicate a cumulative effect of pretreatments, reflecting the synergistic action of NaOH and H_2O_2, which enhances internal accessibility, facilitates oxidant diffusion, accelerates C2–C3 bond cleavage, promotes secondary reactions, and induces structural disorder, leading to a decrease in cellulose crystallinity.

The obtained results are consistent with those reported by Hao et al. [11]. Therefore, it can be concluded that the type of pretreatment governs the accessibility of the oxidant and the oxidation pathway, while the decrease in X_c induced by $NaIO_4$ oxidation results from the cleavage of C2–C3 bonds within the AGU, secondary reactions, and the progressive weakening and fragmentation of the crystalline architecture of cellulose.

3.2. The Determining Role of Pretreatments on the Mechanical, Hydrophilic, and Optical Behavior of Cotton Fabrics Oxidized with $NaIO_4$

3.2.1. Analysis of the Mechanical Behavior of $NaIO_4$–Oxidized Cotton Fabrics as a Function of Applied Pretreatments

Mechanical performance was evaluated using the maximum tensile force at break (Fa) and elongation at break (E), normalized to the corresponding reference sample values (Fa/Fa_0 and E/E_0). Values below unity indicate relative reductions in mechanical properties. Figure 6a,b presents the normalized variations in Fa/Fa_0 and E/E_0 as a function of pretreatment route and oxidation severity. All percentage variations are reported relative to the corresponding reference samples.

The normalized mechanical data (Figure 6) reveal a transition from controlled oxidation to pronounced structural degradation in agreement with data reported in the literature [20,27]. The significant decrease in tensile strength and elongation is attributed to the extensive cleavage of the C2-C3 bonds. This structural disintegration, highlighted by the transition to secondary oxidation products (carboxyl groups, intramolecular cyclic carbonyl structures, e.g., hemiacetal and lactone forms), leads to severe depolymerization and increased fiber brittleness. Therefore, the decrease in mechanical properties is primarily associated with cleavage of glycosidic bonds, disruption of the hydrogen-bond network, and partial depolymerization induced by periodate oxidation and subsequent secondary reactions [32].

SC samples oxidized with 0.04 mol·L^{-1} $NaIO_4$ (30–40 °C) show the best preservation of mechanical properties, compared to the BC and SBC series, with Fa/Fa_0 reductions limited to 41–55% (warp) and 45–52% (weft), while E/E_0 remains largely preserved (−8 to −9%) or slightly increased in the weft direction (+1–7%). This behavior is consistent with predominantly primary oxidation and DAC formation, with limited macromolecular degradation.

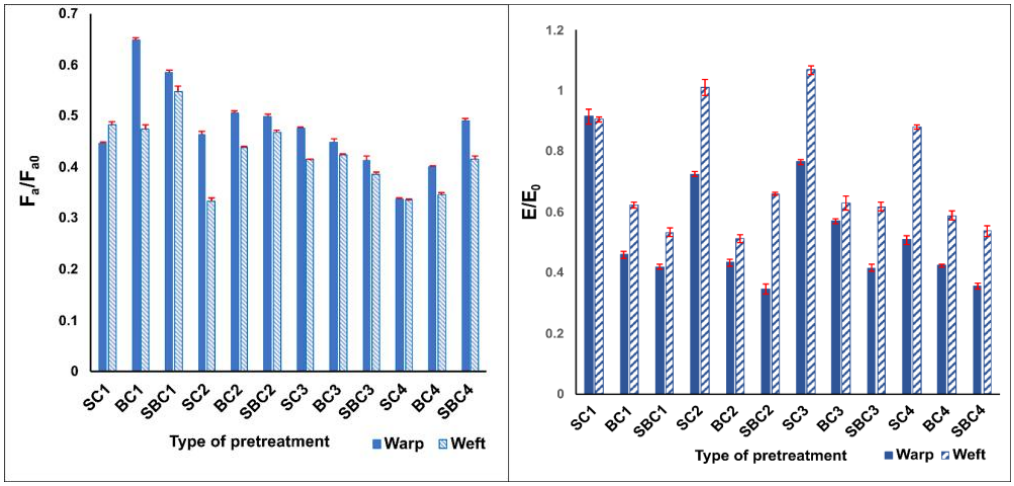

(**a**) (**b**)

Figure 6. Variation in normalized mechanical parameters as a function of pretreatment route: (**a**) Fa/Fa_0 in the warp and weft directions; (**b**) E/E_0 in the warp and weft directions. Values are expressed as normalized fractions relative to the corresponding reference samples (F/F_0 and E/E_0). Error bars represent the propagated standard deviation of the Fa/Fa_0 and E/E_0 ratio (σ_R).

In contrast, the BC series exhibits a balanced mechanical response, with moderate Fa/Fa_0 reductions (~35% for BC1) at mild conditions, and more pronounced decreases (50–60% for BC2, BC3, and BC4) at higher oxidant concentration and temperature, while E/E_0 remains within a moderate range (34–58%). This evolution suggests the coexistence of primary oxidation and secondary reactions, with partial chain scission compensated by reorganization of the hydrogen-bonding network, thereby preventing excessive embrittlement of the material through the formation of carboxyl groups [27].

Under severe oxidation conditions (0.08 $mol \cdot L^{-1}$ $NaIO_4$ at 40 °C), mechanical degradation becomes significant, with Fa/Fa_0 and E/E_0 decreasing to 51–66% and 49–64%, respectively, indicating advanced structural deterioration.

The pronounced decrease in tensile properties observed after periodate oxidation cannot be explained solely by the moderate reduction in crystallinity revealed by XRD analysis. Although $NaIO_4$ oxidation induces a measurable moderate decrease in the crystallinity index, particularly under severe conditions, the magnitude of this structural change remains relatively limited compared with the drastic loss of mechanical performance. This disproportion indicates that tensile deterioration is mainly associated with molecular scale modifications of cellulose, namely the selective cleavage of the vicinal diol at the C2–C3 positions of the AGU, which introduces localized chain scission defects and disrupts the hydrogen bond network responsible for load transfer within the cellulose microfibrils.

Differences between warp and weft directions reflect fabric anisotropy, with larger reductions observed in the weft direction due to its higher amorphous content and increased oxidant accessibility compared with the more crystalline and aligned warp yarns [56–59].

3.2.2. Evaluation of the Hydrophilicity of Oxidized Cotton Fabrics

Periodate oxidation induced selective C2–C3 cleavage within the AGU, leading to DAC formation, together with secondary aldehyde transformations (hydration, aldal and hemiacetal formation) and carboxyl groups, significantly alters the hydrophilic behavior of cotton fabrics. These chemical changes occur concurrently with supramolecular reorganization of the cellulose structure [41,60]. The literature reports non-uniform trends regarding the effect of $NaIO_4$ oxidation on the water retention value (WRV) of cellulose. Moderate oxidation levels have been associated with increased WRV due to oxidation-

induced amorphization and enhanced water accessibility within less ordered domains [41], whereas advanced oxidation stages frequently lead to decreased water retention as a result of aldehyde mediated intra- and intermolecular crosslinking, network densification, and the progressive loss of effective water adsorption sites [60,61].

Surface-related behavior was evaluated through water absorption capacity (WAC), which reflects the liquid uptake ability of the oxidized cotton fabrics.

Table 4 summarizes the influence of pretreatment route and $NaIO_4$ oxidation severity on cotton fabric hydrophilicity, expressed by the water absorption capacity (WAC) and its relative variation (ΔWAC).

Table 4. WAC and ΔWAC values obtained for the reference samples and $NaIO_4$ oxidized cotton fabrics.

Sample	WAC (%) Mean ± SD, n = 3	ΔWAC %
RC	52.83 ± 0.29	-
SC	128.26 ± 0.70	75.43
BC	125.10 ± 0.48	72.27
SBC	118.77 ± 0.42	65.94
SC1	102.28 ± 0.16	−25.98
BC1	98.22 ± 0.43	−26.88
SBC1	94.29 ± 0.26	−24.48
SC2	90.94 ± 0.15	−37.32
BC2	81.05 ± 0.06	−44.05
SBC2	78.98 ± 0.23	−39.80
SC3	90.96 ± 0.22	−37.30
BC3	85.01 ± 0.41	−40.09
SBC3	87.22 ± 0.38	−31.55
SC4	99.32 ± 1.01	−28.94
BC4	87.92 ± 0.23	−37.18
SBC4	75.09 ± 0.23	−43.68

The data presented in Table 4 highlight the effect of the pretreatment route and $NaIO_4$ oxidation severity on fabric hydrophilicity, as reflected by the water absorption capacity (WAC) and its relative variation (ΔWAC).

The reference samples subjected only to conventional pretreatments exhibit a pronounced increase in WAC compared to RC, reflecting enhanced water accessibility following the removal of hydrophobic waxes. Specifically, WAC increases from 52.83% for the untreated fabric to values exceeding 125% for the SC and BC samples, while the combined scouring–bleaching route yields a slightly lower, yet still markedly elevated, WAC.

$NaIO_4$ oxidation leads to a consistent decrease in WAC across all pretreatment series, reflecting a progressive loss of fabric hydrophilicity. For each oxidized sample, the relative reduction is quantified with respect to its corresponding non-oxidized reference, with ΔWAC values ranging from 24.5% to 44.1%. Among the oxidized fabrics, samples processed under mild conditions (0.04 mol L^{-1} $NaIO_4$ at 30 °C; SC1, BC1, and SBC1) exhibit the most balanced hydrophilic response, showing only moderate reductions in WAC (approximately 24–26%). In contrast, oxidation performed at elevated temperature (40 °C) or higher oxidant concentration (0.08 mol L^{-1} $NaIO_4$) results in markedly larger WAC losses, particularly for BC2, BC3, and SBC4, where reductions approach 44%, indicating a pronounced restriction of water uptake.

In this context, the WAC results obtained in the present study are consistent with literature reports describing decreased water uptake at advanced stages of $NaIO_4$ oxidation. In oxidized cotton fabrics, oxidation-induced chemical modifications prevail over partial amorphization effects: the conversion of secondary hydroxyl groups into aldehyde moieties, their participation in hemiacetal linkages, and the formation of lactonic structures promote network densification, restrict chain mobility, and limit swelling as well as effective hydrogen-bond interactions with water. These combined effects alter the capillary–porous structure of cotton cellulose and result in a systematic decrease in WAC with increasing oxidation severity.

Consequently, mild oxidation conditions (0.04 $mol \cdot L^{-1}$ $NaIO_4$ at 30 °C) applied to SC, BC or SBC oxidized series can be regarded as an acceptable compromise, enabling controlled cellulose functionalization while inducing oxidation-related structural rearrangements that restrict water accessibility. These changes result in a reduced WAC, indicating a moderated interaction between the oxidized cellulose matrix and water.

3.2.3. Evaluation of Optical Properties

The literature reports contradictory findings regarding the molecular origin of yellowing in cellulosic materials, with the relative contributions of aldehydic (–CHO) and carboxylic (–COOH) groups remaining under debate [62]. In cotton fabrics, the degree of whiteness (CIE Whiteness Index, WI_{CIE}) [32] and the yellowness index (YI) [63] are closely related to chemical modifications of cellulose induced by conventional pretreatments and controlled oxidation processes. Although both aldehydic and carboxylic groups have been identified as contributors to yellowing, these functionalities generally coexist in cellulosic materials, and their effects are therefore superimposed rather than independent [62].

Table 5 summarizes the colorimetric coordinates and YI values of cotton fabrics subjected to different pretreatment routes and $NaIO_4$ oxidation.

Table 5. Colorimetric coordinates and yellowness index (YI) of cotton fabrics subjected to different pretreatments and $NaIO_4$ oxidation. The parameter b* represents the yellow–blue coordinate in the CIELab color space.

Sample	b*	X	Y	Z	Yellow Index (YI)
RC	11.3	65.07	67.25	59.09	26.02
SC	10.72	67.94	70.51	62.81	24.09
BC	3.97	76.84	80.41	80.89	9.80
SBC	4.39	76.47	79.99	79.9	10.67
SC1	11.41	68.78	71.61	63.07	24.84
BC1	8.37	72.8	76.39	71.23	17.92
SBC1	7.04	72.46	76.01	72.49	15.51
SC2	10.5	70.56	73.54	65.94	22.88
BC2	7.51	73.21	76.84	72.73	16.27
SBC2	6.85	73.26	76.93	73.65	14.96
SC3	11.5	66.28	68.68	60.22	25.90
BC3	6.17	73.6	77.3	74.87	13.65
SBC3	5.31	73.3	76.86	75.52	12.24
SC4	11.03	70.52	73.62	65.41	23.61
BC4	7.16	73.3	77	73.32	15.51
SBC4	6.49	73.48	77.07	74.24	14.43

The colorimetric coordinates and YI values reported in Table 5 show that the raw reference sample (RC) exhibits the highest yellowness index (YI ≈ 26.0), attributed to the presence of natural pigments and chromophoric impurities inherent to raw cotton. Alkaline scouring results in only a limited reduction in yellowing (SC, YI = 24.1), whereas hydrogen

peroxide bleaching leads to a pronounced decrease in YI for the BC and SBC samples (YI = 9.8–10.7). This decrease is accompanied by increased X, Y, and Z tristimulus coordinates, confirming the formation of a whiter, brighter, and optically more stable substrate.

Correlation of the colorimetric parameters with the YI–$F_{aldehyde}$ relationship (Figure 7) highlights the dominant role of the aldehyde fraction, modulated by pretreatment history, in governing the optical stability of cotton fabrics.

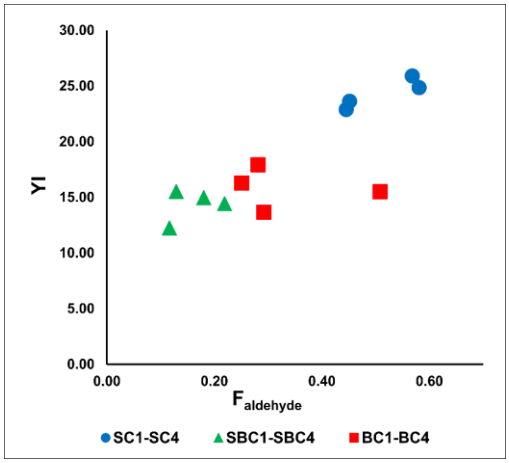

Figure 7. Correlation between the yellowness index (YI) and the aldehyde fraction $F_{aldehyde}$. Symbols represent mean values for each sample. SC1–SC4, BC1–BC4 and SBC1–SBC4 denote individual samples oxidized with $NaIO_4$ at a concentration of 0.04 and 0.08 mol·L^{-1}, at 30 and 40 °C.

Figure 7 demonstrates a direct correlation between the content of optically active free aldehyde groups and the degree of yellowing of cotton fabrics. The SC series (SC1–SC4), characterized by high $F_{aldehyde}$ values (0.45–0.60), exhibits the highest yellowness index values (YI = 22.88–25.90), confirming the dominant role of free aldehydes in the formation of conjugated chromophoric species, as also supported by ATR-FTIR deconvolution results. In contrast, the BC (BC1–BC4) and SBC (SBC1–SBC4) series display lower $F_{aldehyde}$ values (0.12–0.30), corresponding to significantly reduced YI values (12–18) and enhanced optical stability, consistent with ATR-FTIR evidence of modified carbonyl speciation. These results indicate that yellowing is primarily governed by the aldehyde fraction, controlled by pretreatment history and oxidation conditions, while carboxyl groups play a secondary, modulatory role. Accordingly, previously bleached samples retain superior optical stability, even under severe periodate oxidation, due to reduced free aldehyde content and increased formation of masked aldehyde species [32,62].

4. Conclusions

This study investigated how conventional cotton fabric pretreatments, such as alkaline scouring (SC), hydrogen peroxide bleaching (BC) and combined scouring–bleaching (SBC), govern selective sodium periodate oxidation and the resulting structure–property relationships in woven cotton fabrics. Oxidation was performed under controlled conditions (0.04–0.08 mol L^{-1}, 30–40 °C, 4 h and pH 4.0) to enable the evaluation of the combined effects (substrate accessibility and reaction severity) on the chemical, structural, and functional responses of the fabrics.

The results demonstrate that the pretreatment route is the dominant factor controlling oxidant accessibility to the secondary hydroxyl groups at the C2–C3 positions of the AGU and, consequently, the prevailing oxidation pathway. The free aldehyde fraction ($F_{aldehyde}$) varied between 0.13 and 0.58, indicating pronounced pretreatment dependent differences in carbonyl speciation. ATR–FTIR analysis combined with spectral deconvolution confirmed

the formation of carbonyl functionalities in the oxidized cotton fabrics. The characteristic ν(C=O) band at 1730–1740 cm^{-1} confirmed the presence of aldehyde groups, with additional contribution at 1760–1770 cm^{-1} attributed to lactone carbonyl groups. XRD analysis revealed moderate decreases in crystallinity, reaching approximately 24% under severe oxidation conditions, indicating partial preservation of the cellulose Iβ crystalline structure accompanied by increased amorphization. Despite these limited structural changes, mechanical testing showed pronounced deterioration of tensile properties. SC fabrics oxidized under mild conditions retained the highest structural integrity, whereas BC substrates exhibited stronger degradation, with Fa/Fa_0 reductions up to 50–60% and E/E_0 values between 34–58%. These structural modifications were accompanied by a 25–45% reduction in water absorption capacity, reflecting reduced hydrophilicity, particularly for the highly accessible BC and SBC substrates. Optical stability was strongly influenced by the free aldehyde fraction, explaining the pronounced yellowing observed in selectively oxidized SC samples and the improved color stability of pre-bleached substrates.

Overall, the results demonstrate that effective functionalization of woven cotton fabrics by periodate oxidation requires a pretreatment centered strategy in which substrate history governs oxidation pathways, while reaction conditions control the extent of structural modification and functional performance.

Furthermore, this study proposes a methodological framework for interpreting the oxidation behavior of woven cotton fabrics as a function of the applied pretreatment route. The introduction of the free aldehyde fraction ($F_{aldehyde}$) as an indicator of carbonyl speciation, combined with the deconvolution of ATR-FTIR spectra and XRD diffractograms, enabled a more accurate identification of carbonyl species and a more reliable assessment of the structural and functional changes occurring during periodate oxidation.

By integrating chemical quantification, spectroscopic analysis, structural characterization, and functional evaluation, this study establishes a structure–process–property framework for periodate oxidized cotton fabrics. This integrated approach provides a predictive basis for tailoring oxidation conditions to specific cotton fabric applications, through controlled functionalization, limitation of substrate degradation, and optimization of required functional properties.

Author Contributions: Conceptualization, R.P., M.P. and S.S.M.; methodology, R.P., M.P., V.P., V.V. and D.E.C.; software, S.S.M. and R.P.; validation, R.P., V.P., M.P. and D.T.; formal analysis, R.P. and D.E.C.; investigation, R.P., M.P., V.V. and S.S.M.; resources, M.P., V.P. and D.E.C.; data curation, R.P., V.P., M.P., V.M. and S.S.M.; writing—original draft preparation, R.P., M.P., V.M. and S.S.M.; writing—review and editing, M.P., R.P., V.P., S.S.M. and D.E.C.; visualization, R.P. and S.S.M.; supervision, M.P., S.S.M. and V.P.; project administration, R.P. and V.P.; funding acquisition, V.P. All authors have read and agreed to the published version of the manuscript.

Funding: This research was funded by the Doctoral School of the "Gheorghe Asachi" Technical University of Iasi, Romania, based on M.E.C order No. 7048/22.12.2025 valid for doctoral research starting in 2026.

Data Availability Statement: The raw data supporting the conclusions of this article will be made available by the authors on request.

Acknowledgments: The authors acknowledge the logistic support offered by the Centre for Research and Innovation in Textiles and Fashion Industry—SMARTTex-IS.

Conflicts of Interest: The authors declare no conflicts of interest. The funders had no role in the design of this study; in the collection, analyses, or interpretation of data; in the writing of the manuscript; or in the decision to publish the results.

Abbreviations

The following abbreviations are used in this manuscript:

AGU	Anhydroglucose Unit
BC	Bleached cotton
^{13}C-NMR	Carbon-13 Nuclear Magnetic Resonance
DAC	Dialdehyde cellulose
ATR-FTIR	Attenuated Total Reflectance-Fourier Transform Infrared Spectroscopy
NIR	Near-Infrared Spectroscopy
RC	Raw cotton
SC	Scoured cotton
SBC	Scoured and bleached cotton
TEMPO	2,2,6,6-Tetramethylpiperidine-1-oxyl
WAC	Water Absorption Capacity
WRV	Water Retention Value
XRD	X-ray Diffraction
YI	Yellowness Index

References

1. Moon, R.J.; Martini, A.; Nairn, J.; Simonsen, J.; Youngblood, J. Cellulose nanomaterials review: Structure, properties and nanocomposites. *Chem. Soc. Rev.* **2011**, *40*, 3941–3994. [CrossRef] [PubMed]
2. Shi, J.; Zeng, Y.; Liu, C.; Wang, L.; He, J.; Zhang, Y.; Zang, Y.; Zhang, M. Biodegradable, fire-safe, and wearable triboelectric nanogenerator enabled by polyphenol-mediated 1D/2D interface architecture. *Chem. Eng. J.* **2025**, *519*, 164809. [CrossRef]
3. Klemm, D.; Heublein, B.; Fink, H.P.; Bohn, A. Cellulose: Fascinating biopolymer and sustainable raw material. *Angew. Chem. Int. Ed.* **2005**, *44*, 3358–3393. [CrossRef] [PubMed]
4. Nishiyama, Y.; Langan, P.; Chanzy, H. Crystal structure and hydrogen-bonding system in cellulose Iβ from synchrotron X-ray and neutron fiber diffraction. *J. Am. Chem. Soc.* **2002**, *124*, 9074–9082. [CrossRef]
5. Kim, U.J.; Kuga, S.; Wada, M.; Okano, T.; Kondo, T. Periodate oxidation of crystalline cellulose. *Biomacromolecules* **2000**, *1*, 488–492. [CrossRef]
6. Durán, V.L.; Larsson, P.A.; Wågberg, L. Chemical modification of cellulose-rich fibres to clarify the influence of chemical structure on the physical and mechanical properties of cellulose fibres and the sheets made thereof. *Carbohydr. Polym.* **2018**, *182*, 1–7. [CrossRef]
7. Coseri, S.; Biliuta, G.; Simionescu, B.C. Selective oxidation of cellulose with periodate: Properties and applications. *Carbohydr. Polym.* **2013**, *93*, 207–215. [CrossRef]
8. Liu, X.; Wang, L.; Song, X.; Song, H.; Zhao, J.R.; Wang, S. A kinetic model for oxidative degradation of bagasse pulp fiber by sodium periodate. *Carbohydr. Polym.* **2012**, *90*, 218–223. [CrossRef]
9. Potthast, A.; Kostic, M.; Schiehser, S.; Kosma, P.; Rosenau, T. Studies on oxidative modifications of cellulose in the periodate system: Molecular weight distribution and carbonyl group profiles. *Holzforschung* **2007**, *61*, 662–667. [CrossRef]
10. Vicini, S.; Princi, E.; Luciano, G.; Franceschi, E.; Pedemonte, E.; Bajer, D.; Kaczmarek, H.; Sionkowska, A. Thermal analysis and characterisation of cellulose oxidised with sodium metaperiodate. *Thermochim. Acta* **2004**, *418*, 123–130. [CrossRef]
11. Hao, L.; Wang, R.; Fang, Z. Dialdehyde cellulose-based materials for biomedical applications. *Carbohydr. Polym.* **2018**, *184*, 299–306.
12. Patel, M.; Patel, J.; Kevadiya, B. Biomedical applications of oxidized cellulose. *Carbohydr. Polym.* **2017**, *167*, 34–45. [CrossRef]
13. Shaohua, Z.; Li, J.; Chen, S.; Zhang, X.; Ma, J.; He, J. Oxidized cellulose-based hemostatic materials. *Carbohydr. Polym.* **2020**, *230*, 115585. [CrossRef] [PubMed]
14. Wang, X.; Liu, H.; Chen, X. Cationized cotton with polyethyleneimine for enhanced hemostatic performance. *J. Biomed. Mater. Res. B Appl. Biomater.* **2021**, *109*, 532–540.
15. Su, J.; Liu, C.; Sun, A.; Yan, J.; Sang, F.; Xin, Y.; Zhao, Y.; Wang, S.; Dang, Q. Hemostatic and antimicrobial properties of chitosan-based wound healing dressings: A review. *Int. J. Biol. Macromol.* **2025**, *306*, 141570. [CrossRef]
16. Coradi, M.; Zanetti, M.; Valério, A.; de Oliveira, D.; da Silva, A.; Ulson de Souza, S.M.A.G.; Ulson de Souza, A.A. Production of antimicrobial textiles by cotton fabric functionalization and pectinolytic enzyme immobilization. *Mater. Chem. Phys.* **2018**, *208*, 28–34. [CrossRef]
17. Kramar, A.; Korica, M.; Kostic, M. Comparative analysis of electrokinetic properties of periodate- and TEMPO-oxidized regenerated cellulose fabric functionalized with chitosan. *Textiles* **2024**, *4*, 57–69. [CrossRef]

18. Wen, J.; Almurani, M.; Liu, P.; Sun, Y. Aldehyde-functionalized cellulose as reactive sorbents for the capture and retention of polyamine odor molecules associated with chronic wounds. *Carbohydr. Polym.* **2023**, *316*, 121077. [CrossRef]
19. Guigo, N.; Mazeau, K.; Putaux, J.-L.; Heux, L. Surface modification of cellulose microfibrils by periodate oxidation and subsequent reductive amination with benzylamine: A topochemical study. *Cellulose* **2014**, *21*, 4119–4133. [CrossRef]
20. Nypelö, T.; Berke, B.; Spirk, S.; Sirviö, J.A. Review: Periodate oxidation of wood polysaccharides—Modulation of hierarchies. *Carbohydr. Polym.* **2021**, *252*, 117105. [CrossRef]
21. Sulaeva, I.; Klinger, K.M.; Amer, H.; Henniges, U.; Rosenau, T.; Potthast, A. Determination of molar mass distributions of highly oxidized dialdehyde cellulose by size exclusion chromatography and asymmetric flow field-flow fractionation. *Cellulose* **2015**, *22*, 3569–3581. [CrossRef]
22. Sultana, N.; Edlund, U.; Guria, C.; Westman, G. Kinetics of periodate-mediated oxidation of cellulose. *Polymers* **2024**, *16*, 381. [CrossRef]
23. Coseri, S. Cellulose: To depolymerize. . . or not to? *Biotechnol. Adv.* **2017**, *35*, 251–266. [CrossRef] [PubMed]
24. Brandén, C.M. Determination of the Degree of Oxidation in Dialdehyde Cellulose Using Near Infrared Spectroscopy. Ph.D. Thesis, Karlstad University, Karlstad, Sweden, 2017.
25. Madivoli, E.S.; Gachoki, K.P.; Ngure, G.M.A.; Mutuura, S.; Sujee, M.D. Synthesis and characterization of dialdehyde cellulose nanofibers from *Oryza sativa* husks. *SN Appl. Sci.* **2019**, *1*, 723. [CrossRef]
26. Ding, W.; Zhou, J.; Zeng, Y.; Wang, Y.; Shi, B. Preparation of oxidized sodium alginate with different molecular weights and its application for crosslinking collagen fiber. *Carbohydr. Polym.* **2017**, *157*, 1650–1656. [CrossRef]
27. Toshikj, E.; Jordanov, I.; Dimova, V.; Mangovska, B. Influence of various pre-treatment processes on selective oxidation of cotton yarns. *AATCC J. Res.* **2017**, *4*, 22–28. [CrossRef]
28. Fras Zemljič, L.; Strnad, S.; Šauperl, O.; Stana-Kleinschek, K. Characterization of amino groups for cotton fibers coated with chitosan. *Text. Res. J.* **2009**, *79*, 219–226. [CrossRef]
29. Toshikj, E.; Jordanov, I.; Dimova, V.; Mangovska, B. The Influence of Non-selective Oxidation on Differently Pre-treated cotton yarns. *Mater. Sci. (Medžiagotyra)* **2016**, *22*, 429–434. [CrossRef]
30. Fras, L.; Stana-Kleinschek, K.; Ribitsch, V.; Sfiligoj, M.; Kreze, T. Quantitative determination of carboxylic groups in cellulose by complexometric titration. *Mater. Res. Innov.* **2004**, *8*, 145–146. [CrossRef]
31. Liimatainen, H.; Visanko, M.; Sirviö, J.A.; Osmo, E.O.; Niinimäki, H.J. Enhancement of the nanofibrillation of wood cellulose through sequential periodate–chlorite oxidation. *Biomacromolecules* **2012**, *13*, 1592–1597. [CrossRef]
32. Toshikj, E.; Tarbuk, A.; Grgić, K.; Mangovska, B.; Jordanov, I. Influence of different oxidizing systems on cellulose oxidation level: Introduced groups versus degradation model. *Cellulose* **2019**, *26*, 777–794. [CrossRef]
33. Simon, J.; Tsetsgee, O.; Iqbal, N.A.; Sapkota, J.; Ristolainen, M.; Rosenau, T.; Potthast, A. Fourier transform and near-infrared dataset of dialdehyde cellulose used to determine the degree of oxidation with chemometric analysis. *Data Brief* **2022**, *40*, 107757. [CrossRef]
34. Coseri, S.; Biliuta, G.; Fras Zemljič, L.; Srndovic, J.S. One-shot carboxylation of microcrystalline cellulose in the presence of nitroxyl radicals and sodium periodate. *RSC Adv.* **2015**, *5*, 85889–85897. [CrossRef]
35. Simon, J.; Tsetsgee, O.; Iqbal, N.A.; Sapkota, J.; Ristolainen, M.; Rosenau, T.; Potthast, A. A fast method to measure the degree of oxidation of dialdehyde celluloses using multivariate calibration and infrared spectroscopy. *Carbohydr. Polym.* **2022**, *278*, 118887. [CrossRef] [PubMed]
36. Brault, L.; Marlin, N.; Mortha, G.; Boucher, J.; Lachenal, D. About the assessment of the degree of oxidation of cellulose during periodate reaction: Comparison of different characterization techniques and their discrepancies. *Carbohydr. Res.* **2025**, *552*, 109438. [CrossRef]
37. Calvini, P.; Conio, G.; Princi, E.; Vicini, S.; Pedemonte, E. Viscometric determination of dialdehyde content in periodate oxycellulose. Part. II. Topochemistry of oxidation. *Cellulose* **2006**, *13*, 571–579. [CrossRef]
38. Diankova, S.; Doneva, M. Analysis of oxycellulose obtained by partial oxidation with different reagents. *Bulg. Chem. Commun.* **2009**, *41*, 391–396.
39. Nassif, N.A.A. Effect of different wet processing stages on physical properties of cotton woven fabrics. *Fibres Text.* **2019**, *4*, 13–18.
40. Nikolic, T.; Kostic, M.; Praskalo, J.; Pejic, B.; Petronijevic, Z.; Skundric, P. Sodium periodate oxidized cotton yarn as carrier for immobilization of trypsin. *Carbohydr. Polym.* **2010**, *82*, 976–981. [CrossRef]
41. Wang, J.; Wang, Y.; Liu, Z.; Shao, X.; Lin, Y.; Song, W.; Xu, D.; Gao, Y.; Han, J. Modification methods effects on characteristics of carboxylated cellulose fibers: Carboxyl group introduction method versus physical properties. *BioResources* **2024**, *19*, 1590–1601. [CrossRef]
42. *SR EN ISO 7211-2:2024*; Textiles—Woven Fabrics—Construction—Methods of Analysis—Part 2: Determination of Number of Threads per Unit Length. Romanian Standards Association (ASRO): Bucharest, Romania, 2024.
43. Bulsink, P. PlotFTIR: Plot FTIR Spectra; R Package Version 1.2.1. 2025. Available online: https://cran.r-project.org/web/packages/PlotFTIR/index.html (accessed on 28 December 2025).

44. R Core Team. *R: A Language and Environment for Statistical Computing*; R Foundation for Statistical Computing: Vienna, Austria, 2025; Available online: https://www.R-project.org/ (accessed on 28 December 2025).
45. Wojdyr, M. Fityk: A general-purpose peak fitting program. *J. Appl. Crystallogr.* **2010**, *43*, 1126–1128. [CrossRef]
46. Frerebeau, N. *alkahest: Pre-Processing XY Data from Experimental Methods*; R Package Version 1.3.0; Université Bordeaux Montaigne: Pessac, France, 2025. Available online: https://zenodo.org/records/14927537 (accessed on 28 December 2025).
47. Murthy, N.S.; Minor, H. General procedure for evaluating amorphous scattering and crystallinity from X-ray diffraction scans of semicrystalline polymers. *Polymer* **1990**, *31*, 996–1002. [CrossRef]
48. Ciolacu, D.; Ciolacu, F.; Popa, I.V. Amorphous Cellulose-Structure and Characterization. *Cellulose Chem. Technol.* **2011**, *45*, 13–21.
49. *ISO 13934-1:2013*; Textiles—Tensile Properties of Fabrics—Part 1: Determination of Maximum Force and Elongation at Maximum Force Using the Strip Method. International Organization for Standardization: Geneva, Switzerland, 2013.
50. *ISO 20158:2018*; Textiles—Determination of Water Absorption Time and Water Absorption Capacity. International Organization for Standardization: Geneva, Switzerland, 2018.
51. *ASTM E313-20*; Standard Practice for Calculating Yellowness and Whiteness Indices from Instrumentally Measured Color Coordinates. ASTM International: West Conshohocken, PA, USA, 2020.
52. Calvini, P.; Gorassini, A.; Luciano, G.; Franceschi, E. FTIR and WAXS analysis of periodate oxycellulose: Evidence for cluster mechanism of oxidation. *Vib. Spectrosc.* **2006**, *40*, 177–183. [CrossRef]
53. Nandiyanto, A.B.D.; Ragadhita, R.O.R. How to read and interpret FTIR spectroscope of organic material. *Indones. J. Sci. Technol.* **2019**, *4*, 97–118. [CrossRef]
54. Röhrling, J.; Potthast, A.; Rosenau, T.; Sixta, H.; Kosma, P. Determination of carbonyl functions in cellulosic substrates. *Lenzing. Berichte* **2002**, *81*, 89–97.
55. French, A.D. Idealized powder diffraction patterns for cellulose polymorphs. *Cellulose* **2014**, *21*, 885–896. [CrossRef]
56. Siller, M.; Amer, H.; Bacher, M.; Roggenstein, W.; Rosenau, T.; Potthast, A. Effects of periodate oxidation on cellulose polymorphs. *Cellulose* **2015**, *22*, 2245–2261. [CrossRef]
57. Shet, R.T.; Yabani, A.M. Crease-recovery and tensile-strength properties of cotton cellulose. *Text. Res. J.* **1981**, *51*, 740–744. [CrossRef]
58. Pan, N.; Kovar, R.; Kamali Dolatabadi, M.; Wang, P.; Zhang, D.; Sun, Y.; Chen, L. Origin of tensile strength of a woven sample cut in bias directions. *R. Soc. Open Sci.* **2015**, *2*, 140499. [CrossRef]
59. Madhushree, M.; Vairavel, P.; Mahesha, G.T.; Subrahmanya Bhat, K. A comprehensive review of cellulose and cellulose-based materials: Extraction, modification, and sustainable applications. *J. Nat. Fibers* **2024**, *21*, 2418357. [CrossRef]
60. Nikolic, T.; Kostic, M.; Praskalo, J.; Petronijevic, Z.; Skundric, P. Sorption properties of periodate oxidized cotton. *Chem. Ind. Chem. Eng. Q.* **2011**, *17*, 367–374. [CrossRef]
61. Han, S.; Lee, M.; Kim, B.K. Crosslinking reactions of oxidized cellulose fiber. I. Reactions between dialdehyde cellulose and multifunctional amines on lyocell fabric. *J. Appl. Polym. Sci.* **2010**, *117*, 682–690. [CrossRef]
62. Ahn, K.; Zaccaron, S.; Zwirchmayr, N.S.; Hettegger, H.; Hofinger, A.; Bacher, M.; Henniges, U.; Hosoya, T.; Potthast, A.; Rosenau, T. Yellowing and brightness reversion of celluloses: CO or COOH, who is the culprit? *Cellulose* **2019**, *26*, 429–444. [CrossRef]
63. Milanovic, J.; Schiehser, S.; Potthast, A.; Kostic, M. Stability of TEMPO-oxidized cotton fibers during natural aging. *Carbohydr. Polym.* **2020**, *230*, 115587. [CrossRef]